Development of a patient-specific FE model of the knee to study cartilage degeneration following ACL reconstruction

A sensitivity analysis to evaluate the effects of cartilage and meniscal Young's moduli on cartilage degeneration

M. Talsma

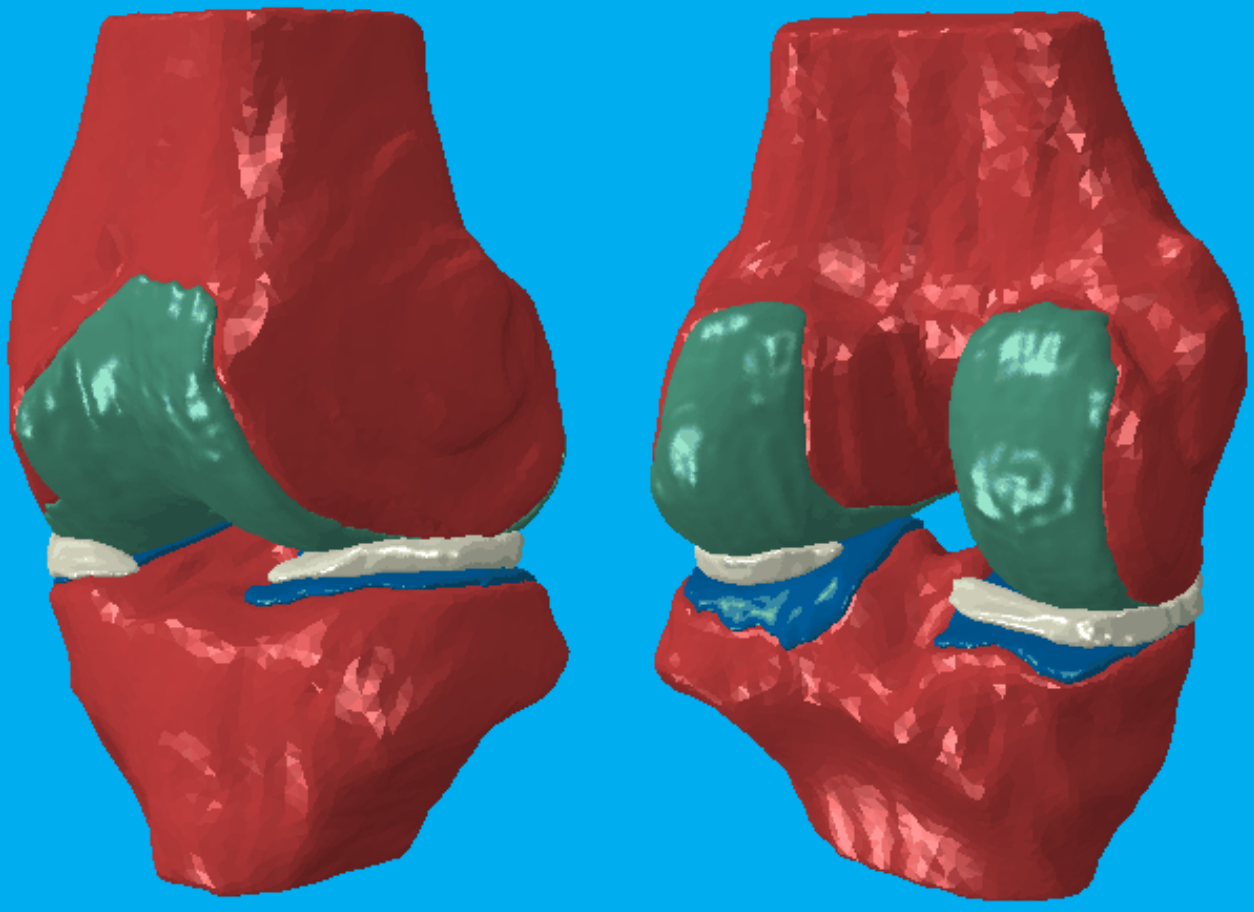

TU Delft

Development of a patient-specific FE model of the knee to study cartilage degeneration following ACL reconstruction

A sensitivity analysis to evaluate the effects of cartilage and meniscal Young's moduli on cartilage degeneration

by

M. Talsma

to obtain the degree of Master of Science in Biomedical Engineering
at the Delft University of Technology,
to be defended publicly on 23-08-2023

Student number: 5412382

Thesis committee:	Dr. ir. N. Tümer,	TU Delft, Supervisor
	Dr. M. G. H. Wesseling,	TU Delft, Daily supervisor
	Prof. dr. ir. J. Harlaar,	TU Delft
	B. Fereidoonnezhad,	TU Delft

TU Delft

Preface

Early on in high school I already knew what I wanted to be growing up, and how to get there; I would study Human Movement sciences and become a rehabilitation therapist. However, when I was finishing up my Bachelor's in Human Movement sciences, I realized this was not the path for me. Becoming an Engineer had never crossed my mind, but at that moment I decided to take a leap and find a new challenge in a new city; Biomedical Engineering in Delft.

I was immediately intrigued by the new approach to my interest in the human body and health. Instead of a scientific approach, I could try to contribute to healthcare by implementing technical solutions. The step to an Engineering Master's was a big one and definitely challenging at times. I can now say I am proud to see how three years later I have almost completed this challenge.

The biggest part of this journey was of course this thesis project, which I could never have successfully completed without the help of others. I would like to start by expressing my gratitude to Mariska Wesseling for your guidance and daily supervision. Every day you were willing to make time for me. Your directions, feedback, and support guided me through my project and motivated me when I was lost at. When you were about to go on maternity leave, you provided me with the right handles to continue my project. Also, I want to thank Nazli Tümer for all your feedback during our (bi)weekly meetings. Your expertise in Finite Element modeling and critical thinking stimulated and enabled me to improve my model step by step. Additionally I want to acknowledge Prof. Jaap Harlaar for your insightful questions and encouragements during the biweekly progress meetings.

Last but not least, I would like to express how grateful I am for my family and friends. Thank you for your constant support and always believing in me.

M. Talsma
Delft, July 2023

Abstract

Osteoarthritis (OA) is a progressive joint degeneration disease resulting in joint pain, stiffness, and loss of mobility. Among patients with anterior cruciate ligament reconstruction (ACLR), OA incidence is increased. Articular cartilage (AC) degeneration is irreversible, therefore prevention and early detection are essential. Specifically, the possibility to predict the risk of AC degeneration would provide options for patient-specific early interventions.

This thesis presents a Finite Element (FE) workflow for a patient-specific FE knee model of a patient with ACLR. A degeneration algorithm is implemented to predict AC degeneration. Uncertainties in the parameters of a FE workflow can affect the model's outcome. The sensitivity of the workflow to the AC and meniscal Young's moduli should be determined, as these influence the stress distribution in the joint but in-vivo measurement is not possible for patient-specific values. Therefore, the developed FE knee model is used to answer the main research question: how sensitive is the predicted AC degeneration of a patient-specific Finite Element ACL reconstructed knee model to changes in the AC and meniscal Young's moduli?

The FE knee model was created based on patient-specific MRI and gait analysis data. For the sensitivity analysis, 24 models were simulated with AC and meniscal Young's moduli varying between 5 MPa and 35 MPa, and 59 MPa and 80 MPa, respectively. A degeneration algorithm was implemented for the calculation of AC degeneration, based on max principal stresses.

Minimal AC degeneration was calculated for both the tibial AC and the femoral AC, ranging from no degeneration to a degeneration level of 0.9812, and 0.9694, respectively. The 5-year follow-up MRI showed no AC degeneration either. Statistical analysis was performed with the volume of degenerated AC. A multiple regression analysis showed an exponential relationship between the degenerated volume and the AC Young's modulus for the tibial AC (R^2 = 0.995, p<0.05), and the femoral AC (R^2 = 0.989, p<0.05). The meniscal Young's modulus did not affect the degenerated volume. The sensitivity analysis demonstrated that increasing AC Young's modulus resulted in a exponentially larger volume of degeneration.

In conclusion, the established FE workflow showed promise for the calculation of AC degeneration following ACLR. A foundation was laid for future development of the model. The sensitivity of the workflow to the AC Young's modulus was determined, highlighting the need for patient-specific estimation of the AC Young's modulus for reliable patient-specific AC degeneration results.

Contents

List of abbreviations

List of Figures

List of Tables

1 Introduction

The human body has the exceptional ability to heal itself. A cut on the finger or a broken leg can be healed within a reasonable amount of time. A band-aid for a day or a cast for six weeks, and the damage is miraculously repaired. Even the entire human skin renews itself approximately every 27 days [1]. The body is capable of a lot of healing, but the ability to regenerate damage to Articular Cartilage (AC) is very limited. AC is devoid of blood vessels, lymphatics, and nerves [2]. Due to the lack of blood vessels, the needed components to restore damage repair cannot be delivered to the damaged tissue site, resulting in the limited healing abilities of the AC. These limited healing abilities imply that damage to the AC is irreversible. This AC damage commonly develops into Osteoarthritis (OA). OA is a progressive joint degenerative disease inducing symptoms such as joint pain, joint stiffness, and ultimately physical disability. Affecting a broad population worldwide, OA is a large burden on healthcare systems [3]. Because of the lack of blood vessels, administration of medication does not reach the damaged target sites in the AC. Therefore, pharmaceutical treatment options have been insufficient to treat OA. Physical therapy is the golden standard for treatment options and focuses on strength and stability training of the joint's surrounding muscles. However, physical therapy can only decelerate the degeneration progress and delay the need for surgery. Also, it is not always effective for all patients. The only solution for end-stage OA is joint arthroplasty. Replacing the damaged joint with an artificial joint is an invasive procedure only used as a last resort.

Risk factors for AC degeneration can be characterized by modifiable and unmodifiable factors [3]. Unmodifiable factors, such as genetic predisposition, gender, and age, are factors that are unchangeable. The most prevalent risk factor is the unmodifiable factor, age [4]. The incidence of OA increases with age, which results in OA being the most common condition among the elderly. Modifiable risk factors such as obesity and injuries to the joint can cause younger people to become susceptible to AC degeneration earlier on in life. As a consequence, injuries of the Anterior Cruciate Ligament (ACL) result in a higher prevalence of OA [5].

One of the functions of the ACL is to stabilize the knee joint. The stabilization is essential for the natural biomechanical behavior of the knee. Injuries to the ligament can result in changes in the biomechanical behavior of the joint, such as an increase in internal rotation during gait or changes in contact pressure distribution on the AC [6]. These abnormal biomechanics are thought to play an important role in the increased susceptibility to AC degeneration, seen in patients with ACL injuries. Treatment options for ACL injuries such as rupture, include ACL Reconstruction (ACLR). However, it has been shown that ACLR often does not fully recover the abnormal biomechanics [7] and even after ACLR, patients are more susceptible to OA. As these patients are usually relatively young and usually do not have AC damage at the time of injury, prevention is essential to avoid the possible development of OA.

In-vivo research methods allow for the estimation of kinetic and kinematic parameters through motion analysis. In-vivo measurement of loading distributions in the knee, on the other hand, is not possible in a non-invasive way. Computational modeling has become a promising field of study to measure internal stresses. Finite Element (FE) analysis is a method frequently applied to computationally model the knee to calculate stresses and strains in the joint [8, 9].

When developing a FE model of a biological system such as the knee, many parameter values

are based on assumptions due to the impossibility to measure these values in-vivo (e.g. tissue material properties, or tissue interaction). In literature, the majority of the FE knee models base these assumptions on other literature or cadaver studies. However, the reliability of these assumptions is usually not validated and the effect of these assumptions on the model's outcome remains unknown.

As mentioned, patient-specific knowledge of knee biomechanics, stress levels, and stress distribution, could be of great importance in the prediction of AC degeneration and therefore a more patient-specific approach to physical therapy. FE analysis can provide valuable information in terms of cartilage stress. Even prediction of AC degeneration is possible when implementing a degeneration algorithm in the model. Degeneration algorithms have been implemented in knee FE models. In literature however, these models are usually incomplete [10, 11], overly simplified [12, 11], and/or are not patient-specific [10, 12, 13]. Ideally, a FE knee model for the prediction of AC degeneration following ACLR is patient-specific, provides reliable results (in terms of stress levels and distribution, and degeneration prognosis), and provides these results within minimum time. The latter is an important factor for the application in clinical settings. Clinicians do not have the time to create a new FE knee model for every patient, making it impossible to use FE modeling for all patients. Therefore, a template FE knee model should be created into which patient-specific parameters can be implemented for a patient-specific analysis. A template FE model is a complete FE base model with generic parameters, besides the patient-specific parameters that need to be implemented. Generic parameter values of the template model are usually based on literature. However, literature shows wide ranges in many of these parameters. The effect of changing model parameters on a FE model's outcome is usually unclear. The sensitivity of a model to these parameters should be tested to understand the impact of the parameter on the cartilage stresses, and thus the AC degeneration prognosis. Material properties vary widely in literature. Within linear elastic models, the value of Young's moduli ranges widely as well [12, 14, 15, 16]. The Young's modulus influences the material's ability to deform under a certain load. In FE knee model, the Young's modulus of the AC is an important factor that affects stress levels of the joint's cartilage to knee loads. As the menisci act as a force damper in between the tibial and femoral AC, changes in the meniscal Young's moduli can affect stress responses in the AC.

The main objective of this thesis is to create a multiscale workflow for a patient-specific FE knee model of a patient with ACLR and implement a degeneration algorithm for the prediction of AC degeneration. The main research question of this thesis will be answered with the created FE knee model; how sensitive is the predicted cartilage degeneration of a patient-specific Finite Element ACL reconstructed knee model to changes in the articular cartilage and meniscal Young's moduli?

2

Method

Within FE analyses, the system of interest is discretized into many smaller parts, called finite elements. Subsequently, a set of algebraic equations can be solved to determine unknown displacements at discrete nodes in structural analysis. These equations are commonly performed by a FE software, such as Abaqus [17]. Thereafter, stresses, strains, and other output parameters can be calculated [18]. A typical FE workflow consists of 3 main phases; a pre-processing, processing, and post-processing phase [19]. A simplified overview of the global components of an FE workflow is shown in Figure 2.1. Pre-processing starts with the segmentation of the images, most commonly Magnetic Resonance Imaging (MRI), to retrieve the geometry of the parts that will be included in the model. Next, the geometry is meshed and material properties are assigned, after which loading and boundary conditions are applied, and interactions are defined. The loading and boundary conditions of the current model are derived from musculoskeletal modeling. A degeneration algorithm is implemented in the model for the AC degeneration prediction. In the processing step, all pre-processed parameters are combined in Abaqus. Post-processing of the FE model focuses on data analysis, followed by checking the validity of the data through comparison with experimental data, or literature. An overview of the workflow created in this thesis is presented in Appendix A. The current chapter will go over the steps in the order of implementation.

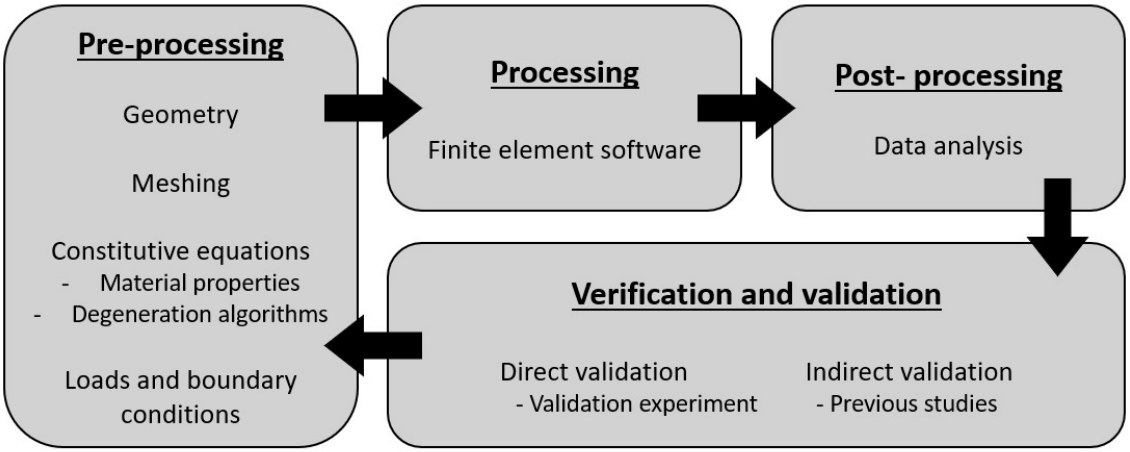

Figure 2.1: General FE workflow.

2.1. Data acquisition

For the patient-specificity of the FE knee model, patient-specific MRI and gait analysis data were used as a basis for the model. MRI and gait analysis data were provided by the Culvenor's group

[20] from the KOALA cohort in Australia [21, 22, 23]. The MRI data were acquired at Olympic Park, Australia. The images were acquired using a 3.0 T MR scanner (Philips Achieva, NL) [21]. Proton Density-weighted (PD) 3d Vista MRI images were used for segmentation with the following acquisition parameters; scanning sequence: Spin Echo (SE), with Segmented K-space (SK), echo time: 27.325 ms, repetition time: 1300 ms, slice thickness: 0.7 mm, spacing between slices: 0.35 mm, imaging frequency: 127.8 MHz. Gait analysis data was acquired at the University of Melbourne, Australia. A walking trial was performed, where the participant was instructed to walk at her natural pace up and down the capture zone.

The participant was a 21-year-old female, weighing 60 kg at the time of baseline MRI and gait analysis (November 2010). The patient underwent ACLR surgery of the left knee in October 2010 after injury, which occurred in June 2010. The ACL was reconstructed using a single bundle 4-strand semitendinosus and gracilis graft. A follow-up MRI was performed 5 years after the baseline MRI. The patient weighed 65 kg at the time of follow-up MRI, this was a small weight gain compared to baseline and was not expected to influence the knee joint forces significantly. Other than an increased echo time of 36.588 ms, compared to 27.325 ms for the baseline MRI, all settings were the same. The echo time is the time between the radio pulse being sent out and the signal echo being measured [24]. There is no significant difference in signal intensity between 36 and 27 ms echo time [25].

2.2. Segmentation

Segmentation of the baseline MRI was performed in 3D slicer (4.8.1) [26, 27]. The images from the different view angles (axial, sagittal, coronal) were aligned by rotating the image slices so the axes of the slices aligned with the segmentation axis to avoid striping artefacts [28].

The FE knee model included the femoral and tibial bones, the femoral and tibial AC, and both menisci as seen in Figure 2.2. Even thought the ligaments were not included as constitutive models, segmentation was performed to determine the origin and insertion sites of the ACLR, Posterior Cruciate Ligament (PCL), Lateral Collateral Ligament (LCL), and Medial Collateral Ligament (MCL). For the segmentation, various tools in the segment editor of 3D slicer were used [29]. For each segment of interest, segmentation was performed using the draw, paint, and erase tools on every 2nd or 3rd slice. The segmented slices were interpolated for the empty slices using the fill-between-slices tool. Segmentations were smoothed using a Gaussian smoothing (window set to 1mm) and shrinking of the segments was avoided using margins. Overlaps between segmentations were corrected using the subtract tool.

2.3. Knee loading and kinematics

Processing of the gait analysis data was performed in OpenSim [30] using the Gait2392 model with 1 Degree of Freedom (DoF) knee [31]. Flexion-extension angle and translational forces were obtained using inverse kinematics, static optimization, and joint reaction analyses [32]. The forces of the femur on the tibia were expressed in the tibial reference frame. The flexion-extension angle in radians was defined as the angle between the femur and tibia, as shown in Figure 2.3. The translational forces in anterior-posterior, medial-lateral, and distal-proximal directions and the flexion-extension angle of the knee were exported. After plotting the raw gait data in Matlab (R2020a), it could be observed that the translational forces showed several non-physiological deviations as seen in Figure 2.4. These deviations and irregularities could cause convergence issues during the simulation in Abaqus. Therefore, the data were smoothed with a Gaussian smoothing window where the window length states the number of data points which were averaged using a Gaussian weighting factor. The window length for increments 1 through 9 was set to 10 for the anterior-posterior force, and 15 for the distal-proximal, and medial-lateral forces. For increments 10 and up, the smoothing window was set to 5 for all translational forces. The difference in window length was applied because the first 9 increments of the data showed large deviations, while the rest of the data did not (Figure 2.4). Applying the same smoothing window would either not be sufficient enough to smooth the large deviations at the start, or flatten the curve too much in the remainder of the data. For the flexion-extension angle, a smoothing window of 3 was used, as the raw data did not show any large deviations. See Appendix B for the used Matlab code. The data comprised one full gait cycle, whereas only the stance phase was included in the FE simulation.

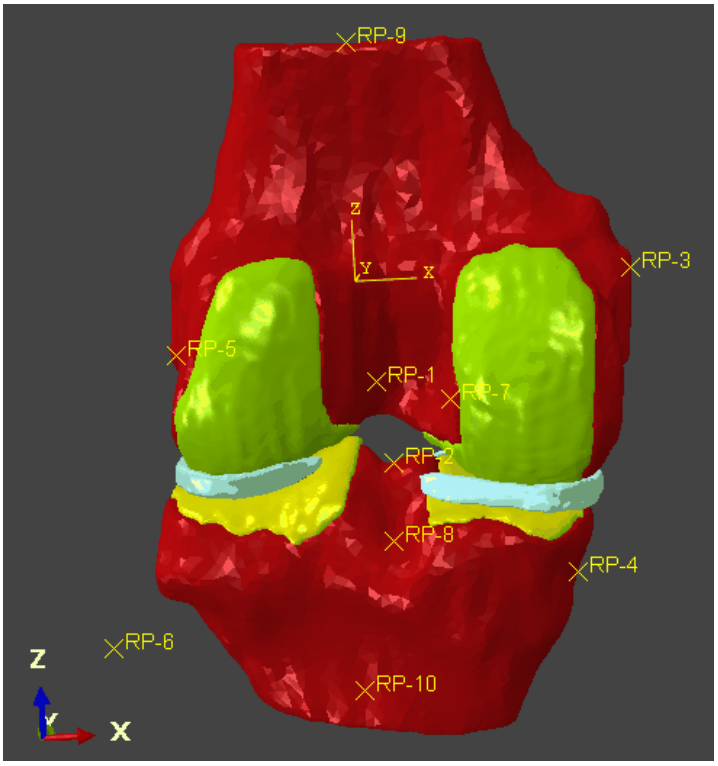

(a) FE model as used in the simulations

RP1	-	ACL origin site
RP2	-	ACL insertion site
RP3	-	MCL origin site
RP4	-	MCL insertion site
RP5	-	LCL origin site
RP6	-	LCL insertion site
RP7	-	PCL origin site
RP8	-	PCL insertion site
RP9	-	RP for femur rigid body
RP10	-	RP for tibia rigid body

(b) Reference points and function

Figure 2.2: Included parts in the FE knee model were the femur, tibia, femoral cartilage, tibial cartilage, and both menisci. Reference points were created to function as the origin and insertion points of the ligaments, modeled as springs.

As most of the cartilage stresses occur during the stance phase of the gait cycle, only this phase was included in the simulation to shorten the computational time. The duration of the stance phase was determined in OpenSim based on the presence of a ground reaction force.

The flexion-extension angle in OpenSim was defined as the rotation of the tibia around the horizontal axis with respect to the femur. The flexion-extension angle in Abaqus was defined as the rotation of the femur with respect to the tibia. Therefore, the rotation was multiplied by -1 when implementing the angle in Abaqus. Furthermore, the tibial local coordinate system of the OpenSim model and the 3D slicer segmented tibia did not align. The center of rotation for the flexion-extension angle was located between the femoral condyles, in the origin of the tibial local coordinate system. To align the local coordinate systems of the models, a transformation matrix was obtained.

The transformation matrix was acquired using 3-matic 16.0 (Materialise). Both the tibia segment, obtained from the 3D slicer segmentation, and the tibia from the OpenSim model were imported into the software. The OpenSim model contained generic segments, resulting in differences between the tibial parts, due to which automatic alignment could not be initiated. Thus, alignment needed to be performed manually. The 3D-slicer tibia segment was rotated and translated such that it aligned with the tibial head of the OpenSim part by 'dragging' the segment. After the alignment of the parts, the transformation matrix was exported. Because the translation/rotation was performed manually and the tibial bones were dissimilar, this method was prone to error due to uncertainty in the accuracy of the alignment. Therefore, the process was performed three times, and the final transformations were averaged over the three trials, which are documented in Appendix C. The patient was scanned in anatomical position, thus the flexion-extension angle was assumed to be 0 radians. All segmented parts were transformed in Abaqus using the transformation matrix of the tibia to preserve the joint alignment. As the femur was segmented from the same scan, there was no transformation matrix created for the femur.

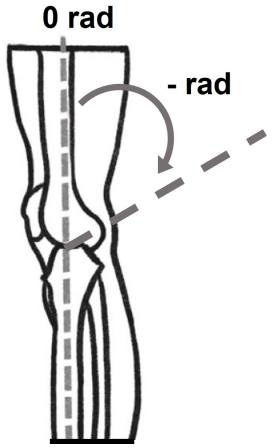

Figure 2.3: The flexion-extension angle in radians was defined as the angle between the femur and tibia. A fully extended knee meant 0 rad, and a decrease in rad when the knee goes in flexion.

Segment	Average edge length [mm]	Number of elements	Number of nodes
Femur	1	12084	6044
Tibia	1	7814	3909
AC femur	0.3	485731	147294
AC tibia	0.2	447155	134474
Lateral meniscus	0.25	66534	20794
Medial meniscus	0.175	198974	60328

Table 2.1: Mesh details per segment of the final model

2.4. Meshing

Segmented knee parts were exported to STL files and meshed using 3-matic 16.0 (Materialise, Leuven, Belgium). The segmented knee tissues were imported in 3-matic as parts and meshed separately. The mesh element sizes were based on a mesh convergence study. All segments were meshed with a uniform tetrahedral mesh with varying target triangle edge lengths per part. The femoral and tibial bones are considered rigid bodies, therefore a volume mesh was not created. The soft tissues were the parts of interest for the current FE knee model and thus needed to contain a volume mesh. The element type was tet4, which are tetrahedral elements with 4 nodes. Tet4 elements are the simplest linear-interpolation tetrahedron-shaped elements to decrease the computational cost of the model.

A mesh convergence study was performed to determine the mesh element size. Ligaments were disregarded for the mesh convergence model for simplicity. A concentrated compression force of 500 N was placed on the femur. The mesh input parameter used was the number of sweep layers of the AC and menisci. The number of sweep layers implied the number of element layers used to create a volume mesh. E.g. for 2 sweep layers, the volume mesh was composed of 2 layers of elements. For the femoral AC and the menisci, 5 different sweep layers were created (2, 3, 4, 5, and 6). The tibial AC was too thin to mesh with 5 or 6 sweep layers, thus the 4-layer sweep was used for these simulations. The main output parameter of the mesh convergence study was the peak max principal stress of the medial and lateral compartments of both AC as this was an important output parameter for the final model as well. The output parameters were assessed in Microsoft Excel (Version 2306). See Appendix D for the included mesh details and convergence results. The output parameter changed less than 5% after sweep layer 4. Therefore, sweep layer 4 was concluded to be the optimal mesh for the final FE model. The corresponding mesh properties are documented in Table 2.1.

Mesh element quality was checked by Abaqus based on a quality measure, minimum interior dihedral angle, and maximum interior dihedral angle. The quality measure was calculated by dividing the volume of a tetrahedron by the volume of an equilateral tetrahedron with the same circumsphere radius. Within the range from 0 for completely distorted, and 1 for equilateral tetrahedron, a quality measure of at least 0.02 was recommended [17]. The interior dihedral angle is the angle between

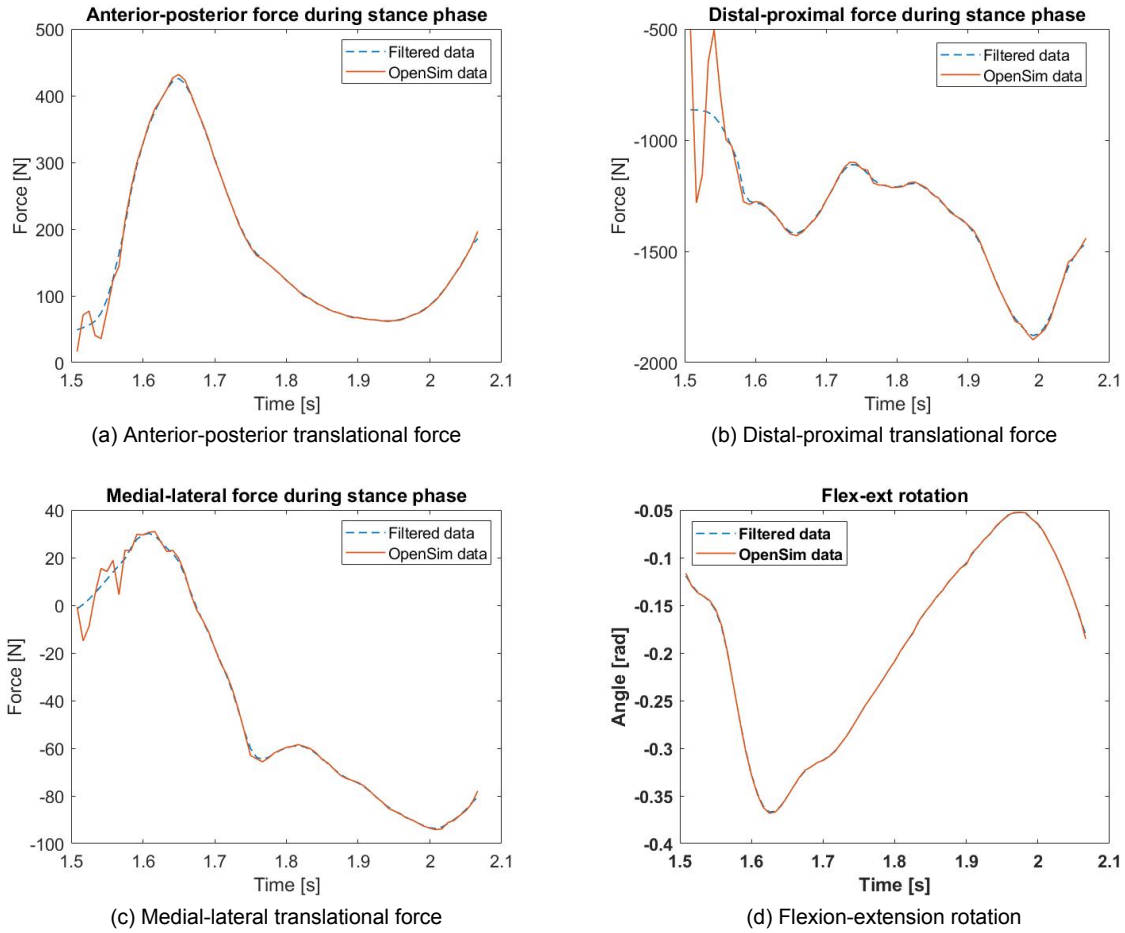

(a) Anterior-posterior translational force

(b) Distal-proximal translational force

(c) Medial-lateral translational force

(d) Flexion-extension rotation

Figure 2.4: Original OpenSim data and smoothed data

2 planes of the tetrahedron. This angle should be between 10°and 160°. If at least one of these parameters did not meet the desired threshold, the element was reported as distorted.

After the mesh convergence study, the soft tissues were exported as volume meshes in an assembly, Abaqus, INP file. The bony parts were exported as STL files. Matlab was used to convert the STL files into SAT files, which allows the bony parts to be imported into Abaqus as discrete rigid parts. The Matlab code used for this conversion is added in Appendix E.

2.5. Assembly

The meshed soft tissues (INP file) were imported in Abaqus as a model, which automatically created an assembly. The femur and tibia were imported as discrete rigid parts and added to the assembly as dependent instance types. Bones were assigned to be rigid because the significant difference in Young's Modulus could be simplified to the bones being rigid compared to the soft tissues [11, 13, 33, 34]. For both the femur and tibia, a Reference Point (RP) was added onto which boundary conditions and loads could be applied for the entire rigid body. A point mass/inertia was created for both rigid bodies, with an isotropic mass of 1 for an evenly distributed mass.

Ligaments were included, and modeled as linear springs. The included ligaments were ACLR, PCL, LCL, and the MCL. An RP was used for every origin and insertion site of the ligaments. Origin and insertion of the ligaments were estimated by importing the segmented ligaments into Abaqus. The coordinates of the RPs were estimated by outlining the edges of the attachment sites and averaging the coordinates. The placements of the RPs can be seen in Figure 2.2. The springs were added between the origin and insertion RPs. Stiffness of the ACLR was set to 200 N/mm, the PCL was set to 120

N/mm, and the MCL and LCL were set to 100 N/mm [35, 36].

After the assembly was created, the entire assembly was transformed using the transformation matrix obtained in Section 2.3.

2.6. Material properties

To assign material properties to the femoral and tibial AC, and the menisci, sections were assigned. Both the AC and the menisci were assigned solid, homogeneous section types. All soft tissues were modeled as linear elastic [37, 33, 38].

2.6.1. Sensitivity analysis

In literature, the material properties of soft tissues show a wide variety [14, 16, 12]. As part of the sensitivity analysis, the Young's moduli of the AC and the menisci were varied based on the found ranges in literature. It was assumed that the femoral AC and tibial AC had the same properties. This assumption was also applied to the medial and lateral menisci. The Young's modulus of the AC ranged from 5 MPa to 35 MPa with 6 intervals [14, 12]. The Young's modulus of the menisci ranged from 59 MPa to 80 MPa with 4 intervals [15, 14, 16]. 24 models were run with combinations of material properties within these ranges as presented in Table 2.2. The material properties for the simulations can be seen in Table 2.2. The Poisson's ratio remained the same for all simulations; 0.45 for the AC and 0.49 for the menisci [38, 16, 15, 14].

The remainder of the model was identical for all simulations to allow for investigation of the sensitivity of the material properties alone.

Model	1	2	3	4	5	6	7	8	9	10	11	12	13	14	15	16	17	18	19	20	21	22	23	24
AC [MPa]	5	11	17	23	29	35	5	11	17	23	29	35	5	11	17	23	29	35	5	11	17	23	29	35
Menisci [MPa]	59	59	59	59	59	59	66	66	66	66	66	66	73	73	73	73	73	73	80	80	80	80	80	80

Table 2.2: Young's Moduli of the AC and menisci of the 24 models included in the sensitivity analysis

2.7. Simulation steps

Abaqus automatically created an initial step in which initial parameters were set for the start of the analysis. Parameters were created in the initial step and remained unchanged throughout the following steps unless mentioned otherwise.

After the initial step, 3 steps were created; a Pre-displacement step, a Pre-load step, and a Gait-cycle step. The time for the pre-displacement step and Pre-load step was left at default; 1 sec (increment sizes, initial: 0.01, minimum: 1E-6, and maximum: 0.1). The Gait-cycle step time was set to match the time of the stance phase; 0.56 sec (increment sizes, initial: 0.01, minimum: 56E-5, and maximum: 0.1). For the Pre-displacement and Pre-load steps, the maximum number of increments was set to 100. The maximum number of increments for the gait-cycle step was set to 1000. Nonlinear effects of deformations and displacements of the geometry (Nlgeom) were allowed. The remaining settings were left at default.

2.8. Contact definitions

To set up the contact properties between parts, the 'finding contact pairs' option of Abaqus was used. This tool automatically finds contacting surfaces within the searched domain (AC and menisci), and assigns a node-to-surface contact. The contact pairs of the current model included:

- Femoral AC - lateral tibial AC
- Femoral AC - medial tibial AC
- Femoral AC - lateral meniscus
- Femoral AC - medial meniscus

- Lateral tibial AC - lateral meniscus
- Medial tibial AC - medial meniscus

An important consideration was determining the master and slave surfaces. In contact pairs where a large size difference in the surfaces can be observed, the larger surface should be assigned the master surface [39]. Thus, for every contact pair including the femoral AC, the femoral AC was assigned the master surface. Between tibial AC and the menisci, the tibial AC was the assigned master surface. A frictionless tangential behavior and a 'hard' contact with normal pressure-overclosure were implemented for all contacting pairs to account for contact behavior in all directions. Node adjustment, slave adjustment, and surface smoothing were turned off to make sure Abaqus did not adjust the position of elements.

2.9. Constraints

Two types of constraints were used for the FE knee model, tie constraints and rigid body constraints. Rigid body constraints were created for the femur and the tibia to allow loads and boundary conditions, applied to a RP, to be applied to the entire rigid body. This RP was placed on the proximal surface of the femur, and the distal surface of the tibia, as shown in Figure 2.2. The rigid body part (femur or tibia) was selected as the body region type and the RP created was selected as the rigid body RP. For the femur, the location of the RP was adjusted to the center of mass at the start of the analysis. The center of mass was automatically calculated based on the assigned inertia, at the beginning of the simulation.

The RPs representing the ligament origins were connected to the femur, using tie constraints. With a tie constraint, the nodes and surfaces tied together experience the same loads and displacements. The discretization method was set to 'node-to-surface'. A rigid body is not allowed to be the slave surface, whereas a node surface should always be the slave surface. Therefore, the RPs were assigned the slave surfaces and the rigid femur was the master surface. The position tolerance specifies a distance from the master surface nodes within which slave surface nodes are tied. Nodes outside the position tolerance are not tied. The position tolerance for the RPs was set to 2 mm to assure the nodes were tied. To prevent adjustment of the initial position of the RPs, this setting was turned off.

Both AC were also connected to the bones using tie constraints. For the tie constraints between AC and the rigid bones, surface-to-surface discretization methods were used. The rigid bodies were selected as the master surface in their tie constraint, again because a rigid body cannot be the slave surface. Therefore, AC was selected as the slave surface and adjustment of the slave surface was not allowed. For tie constraint between AC and bones, the position tolerance was left at default, which based the tolerance region on the average distance between nodes on the master surface.

2.10. Boundary conditions

An encastre boundary condition was applied to the rigid body RP of the tibia. An encastre boundary condition restricts the node of interest of any translation or rotation. Therefore, the tibia was fully constrained from all rotations and translations. As opposed to the origin RPs of the ligaments (located on the femur), the insertion RPs (located on the tibia) were constrained using boundary conditions. The insertion of the LCL is placed on the fibula, which was not included in the current FE Knee model. As the positioning of the springs might affect model results, the RP representing the LCL insertion point was fixed in space at the position where it would have been connected to the fibula (see Figure 2.2, RP-6). All insertion RPs, representing attachment of the ligament to the tibia, were constrained using an encastre boundary condition. The boundary conditions for ligaments, and the tibia were created in the initial step and propagated throughout the following steps without modification.

Furthermore, the menisci needed to be constrained to avoid non-physiological movement. Pressure on the menisci pushes the menisci laterally. In-vivo, the menisci are connected to the tibia via meniscal horns to keep them in place. The current FE model does not contain meniscal horns on account of simplicity. The menisci were constrained at the meniscal horns using an encastre boundary condition as can be seen in Figure 2.5. This boundary condition was also propagated throughout the following steps without modification.

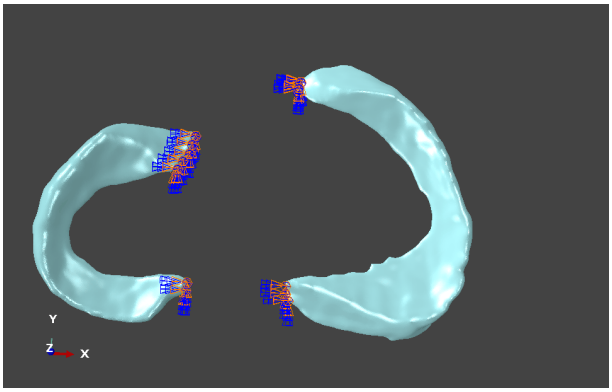

Figure 2.5: An encastre boundary condition was applied where the meniscal horns would be in-vivo

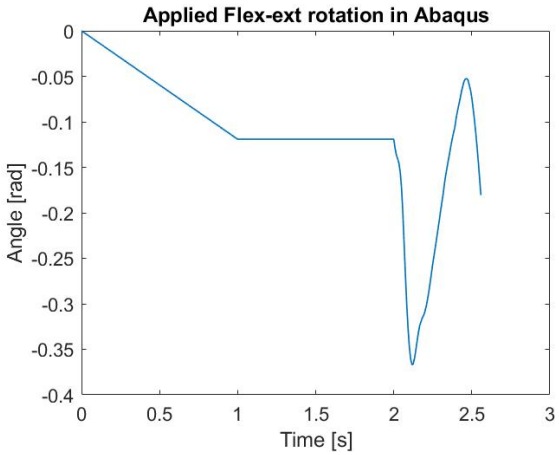

Figure 2.6: Amplitude of the applied flexion-extension angle in Abaqus

The medial-lateral translation and the internal-external rotations were locked using displacement/rotation boundary conditions, while the anterior-posterior translation and superior-inferior translation, and varus-valgus rotation were left open. The flexion-extension angle derived from the patient-specific gait analysis data, was applied as a boundary condition with an amplitude as seen in Figure 2.6. The flexion angle was gradually ramped up to the starting flexion angle of the gait cycle in the Pre-displacement step (0 sec - 1 sec). In the Pre-loading step, the flexion angle was kept constant before initiating a tabular amplitude for the gait cycle in the last step. See Figure 2.7 for the definitions of the translations and rotations.

All boundary conditions acted in the tibial coordinate system.

2.11. Loading conditions

The translational forces were applied as loading conditions. The translational forces were applied as concentrated forces (in Newton) to the RP of the femoral rigid body constraint. In the Pre-load step, the forces were ramped up to the starting value of the loads in the Gait-cycle step. For this step, 3 tabular amplitudes were created for the translational forces. The applied forces can be seen in Figure 2.8.

2.12. Degeneration algorithm

To estimate the degeneration of the femoral and tibial AC, a degeneration algorithm was implemented. The algorithm was based on the degeneration algorithm described by Mononen et al. [40, 10]. The algorithm was implemented using Python (version 2.7) integrated into Abaqus (Appendix F).

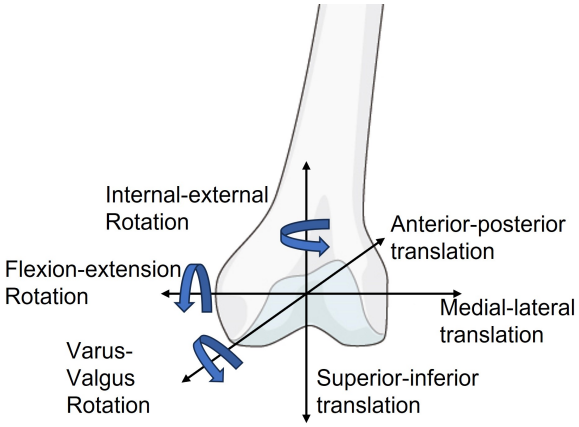

Figure 2.7: An encastre boundary condition was applied where the meniscal horns would be in-vivo

The calculated degeneration represented collagen fibrillation, as this is the first sign of OA [41]. The level of degeneration was calculated for every tetrahedral mesh element of the tibial and femoral AC at every increment, and defined as the total degeneration that occurred over the stance phase of one gait cycle. An increment is defined as a converged increment within the FE analysis. It was assumed that 70% of the degeneration over a longer time period could be estimated with one cycle [41]. The degree of degeneration was assumed to be the consequence of excessive max principal stresses and fatigue following accumulated stress [42]. If the max principal stress of an element surpassed a degeneration threshold value at a specific time increment, a degeneration factor was determined for that increment. The degeneration factor was calculated as:

$$D_{el,i} = \left(\frac{(S_{el}^{i} - T_\alpha)/T_\alpha}{100}\right), \quad if(S_{el,i} > T_\alpha), \tag{2.1}$$

$$D_{el,i} = 0, \quad if(S_{el,i} \leq T_\alpha). \tag{2.2}$$

where $D_{el,i}$ was the degeneration factor of an element at a specific time increment, ranging from 0 to 1 for no degeneration to complete tissue damage, respectively. T_α was the degeneration threshold. If the max principal stress ($S_{el,i}$) was smaller or equal to the degeneration threshold, the degeneration factor would be 0.

In FE calculation, the time per increment (INC_i) is not always the same for every increment (TOT). Therefore, the total degeneration was the weighted sum of the degeneration factor per time increment as stated in Equation 2.3 below.

$$Deg_{el} = 1 - \sqrt[1.5]{\sum_{i=1}^{TOT} D_{el,i} \cdot INC_i} \tag{2.3}$$

The calculated degeneration factor was subtracted from 1 (healthy cartilage), to calculate the final level of degeneration per element,Deg_{el}. When Deg_{el} equaled 1, this represented no degeneration was detected, whereas 0 represented complete cartilage breakdown. The root term index of 1.5 was based on experimental testing done by Mononen et al. (2016) [40]. A nonlinear ramp of degeneration was selected as this showed faster collagen degeneration, comparable to experimentally tested approaches.

The degeneration threshold represents the magnitude of the max principal stress at which cartilage degeneration is initiated. For all 24 simulations, the level of degeneration was calculated using a degeneration threshold of 5 MPa [43].

2.13. Delft High performance computer

Due to extensive simulation time, Abaqus simulations were run in the Delft High performance Computer (DHPC) [44]. The code used to submit the jobs and run the degeneration algorithm called

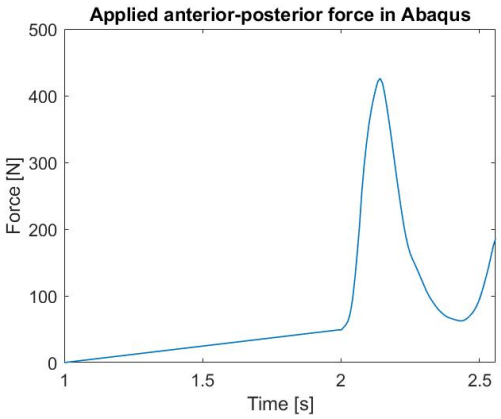

(a) Applied anterior-posterior force

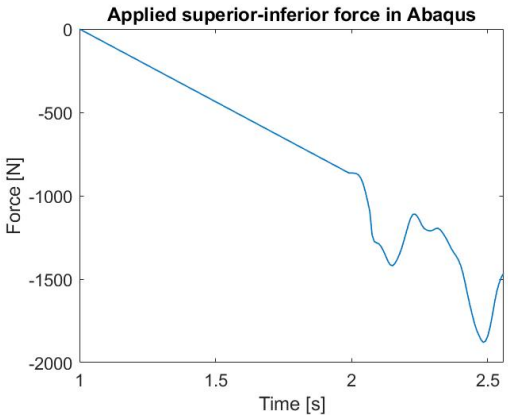

(b) Applied distal-proximal force

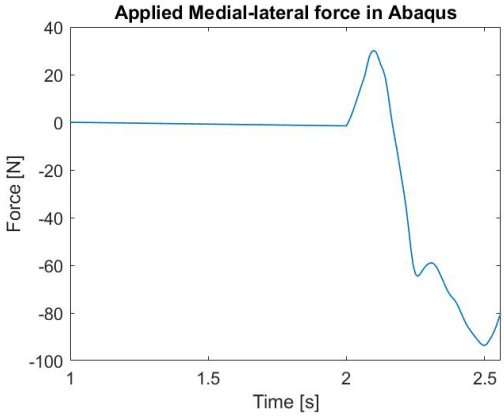

(c) Applied medial-lateral force

Figure 2.8: Original OpenSim data and smoothed data

the batch file, is listed in Appendix G. Per model simulation, 10 Central Processing Unit (CPU)s were allocated to the batch submission. Per CPU, 10G of memory was requested for a total memory of 100G. The time reserved for the job submission was set to 24 hours. For model visualization, access to an Abaqus Graphic User Interface (GUI) was needed. The access was achieved via a visual node on the DHPC. How the connection to the visual node was attained is also listed in Appendix G.

2.14. Post-Processing

As the aim of the created FE knee model was to estimate the degree of cartilage degeneration, the level of degeneration per element was the main output parameter of the model. The main thesis objective was to analyze the sensitivity of the FE model's output to changes in the AC and meniscal Young's moduli. For the sensitivity analysis, the Young's moduli of both menisci and femoral and tibial AC were varied over 24 models (see Section 2.6.1).

The level of degeneration was calculated, using the degeneration algorithm in Section 2.12. The algorithm was based on the max principal stresses calculated in the tibial and femoral AC. Evolving patterns in the stress distributions over the course of the gait cycle were evaluated. This evaluation was performed in the Abaqus visualization module through visual inspection.

Further analyses were performed in MATLAB (R2020a). The level of degeneration of every element per model was presented as histograms for a clear presentation of the differences between models. The degeneration was quantified as the volume of elements that show degeneration AC. The degenerated volume was visualized in figures for both the tibial and femoral AC to observe where degeneration occurred and how the volumes differed between models. For the sensitivity analysis,

		Menisci			
		59	66	73	80
AC	5	N = 1	N = 1	N = 1	N = 1
	11	N = 1	N = 1	N = 1	N = 1
	17	N = 1	N = 1	N = 1	N = 1
	23	N = 0	N = 0	N = 1	N = 1

Table 2.3: Statistical analyses possibilities are limited due to the single sample per independent variable combination. Due to the failure of the models with an AC Young's modulus of 29 MPa and 35 MPa, and two of the models with 23 MPa, these models had a sample size of N=0.

differences in degenerated volume between the models were assessed. Due to the design of the experiment and the single sample per group as seen in Table 2.3, differences were assessed via descriptive parameters and bar graphs instead of statistical tests [45, 46, 47, 48]. The mean degenerated volumes, and ranges were reported to determine the variance in the data.

To determine if there was a correlation between the degenerated volume and the AC and/or meniscal Young's Moduli, multiple regression was used. First, a simple regression was performed to determine the correlation between the degenerated volume and the AC Young's modulus. The exponential equation used for the fit was $f(x) = a * exp(b * x)$. Where f was the dependent variable; degenerated volume, x was the independent variable; the AC Young's modulus, and a and b were the regression coefficients. Second, a multiple exponential regression was performed where the meniscal Young's modulus was added as an independent variable to determine whether the AC and meniscal Young's moduli affected each other and thus improved or decreased the regression with respect to the exponential regression with only the AC Young's modulus. The exponential equation used for the fit of the multiple exponential regression was $f(x1, x2) = a * exp(b1 * x1 + b2 * x2)$. Where $x1$ and $x2$ were the two independent variables, and b1 and b2 were the corresponding coefficients. The coefficients were calculated, and the goodness of the fits of both exponential regressions were determined via the coefficients of determination (R^2) [49]. R^2 ranged between 0 and 1, where a value of 0 indicates that the dependent variable cannot be explained by the independent variable(s) via the exponential model. A value of 1 indicates that the dependent variable is perfectly explained by the independent variable(s) via the exponential model. The results were significant when $p < 0.05$.

3

Results

24 simulations of models with varying material properties, as seen in Table 2.2 were run. Out of the 24 simulations, 10 simulations failed to converge. The models that failed are presented in Table 3.1 with their respected AC and meniscal Young's Moduli. These models were excluded from the statistical analysis. The run time of the completed models in the DHPC was approximately 20 hours per model.

3.1. Max principal stress

The peak max principal stress of the completed models ranged from 2.83 MPa to 9.77 MPa for the tibial AC. These peak stresses were reached between 0.11 sec and 0.12 sec. The peak max principal stress on the femoral AC ranged from 9.72 MPa to 21.82 MPa. These peak stresses were reached at 0.33 sec for all completed models. Max principal stress patterns were similar for all completed models. The highest max principal stress at the first peak of the superior-inferior force in the gait cycle was located posteriorly on the lateral AC, while the highest max principal stress at the second peak of the gait cycle was located anteriorly on the medial AC. The shift was visible on both the tibial and femoral AC. As model 22 showed the highest max principal stress values, the shift for this model is presented in Figure 3.1. The AC and meniscal Young's moduli of model 22 were 23 MPa and 80 MPa, respectively.

3.2. Level of degeneration

First, the level of femoral and tibial cartilage degeneration was estimated using a degeneration threshold of 5 MPa [40]. The calculated level of degeneration per model is shown in Figure 3.2. Only the models that showed any degeneration are presented, and only elements that showed degeneration were included in the figure, including elements with a degeneration level of 0.9999. On the femoral AC of model 1, only 1 element showed degeneration, and in models 7 and 13, only 2 elements showed degeneration. Prior to data analysis, outliers were detected in the distribution of the level of degeneration per model. Both the tibial and femoral AC had one clear outlier. The outlier elements were located on the outer rim of the cartilage layers (see Appendix H). As most degeneration occurs more towards the

Model #	Ac Young's Modulus [MPa]	Meniscal Young's Modulus [MPa]	Time of failure [s] (Total step time: 0.56 s)
4	23	59	0.11
5	29	59	0.10
6	35	59	0.10
10	23	66	0.11
11	29	66	0.10
12	35	66	0.10
17	29	73	0.11
18	35	73	0.10
23	29	80	0.11
24	35	80	0.10

Table 3.1: An overview of the models that did not converge to a solution.

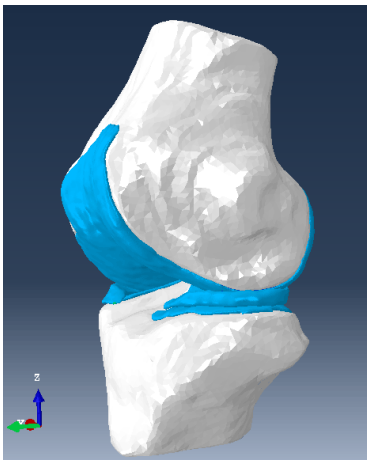

(a) Joint position at the first peak.

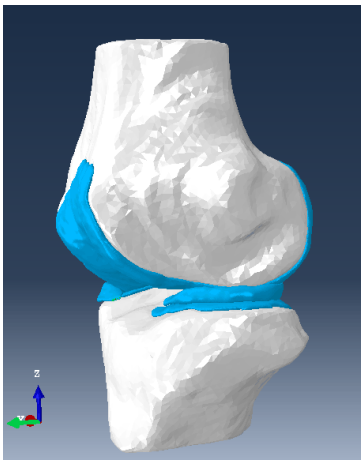

(b) Joint position at the first peak.

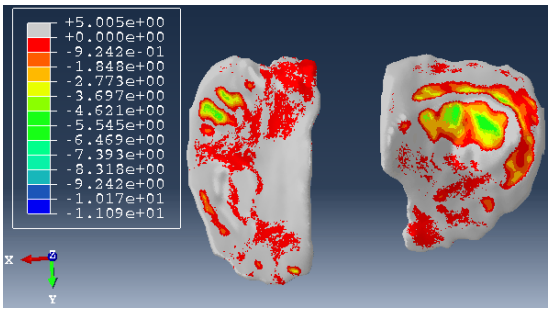

(c) AC tibia at the first peak.

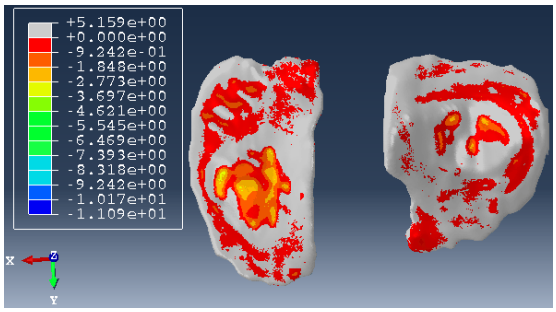

(d) AC tibia at the second peak.

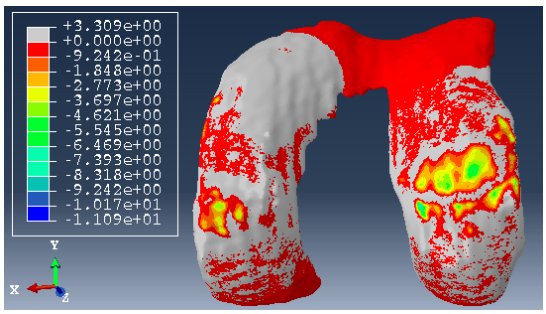

(e) AC femur at the first peak.

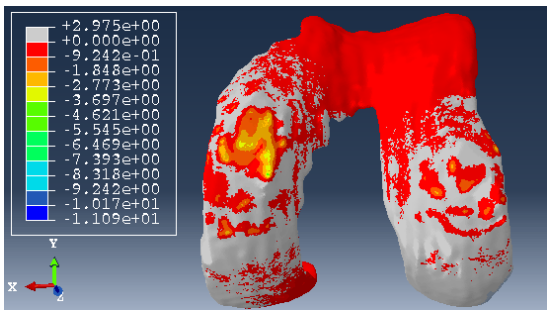

(f) AC femur at the second peak.

Figure 3.1: Shift of the max principal stress [MPa] patterns between the first and second load peak of model 22, aut 0.12s and 0.47s, respectively.

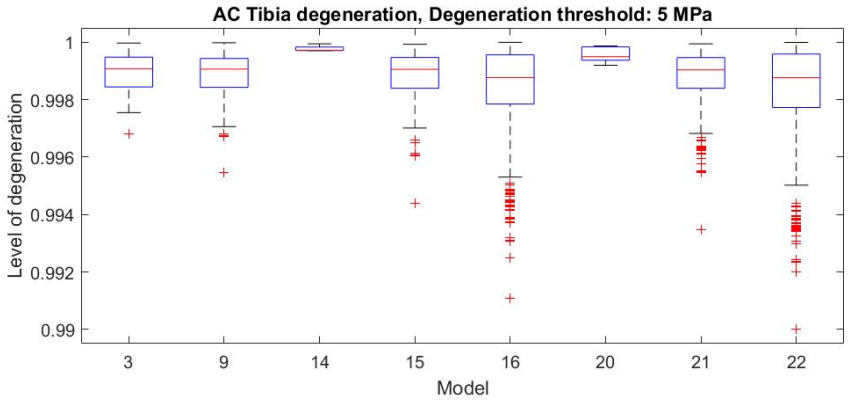

(a) The level of degeneration of the tibial AC.

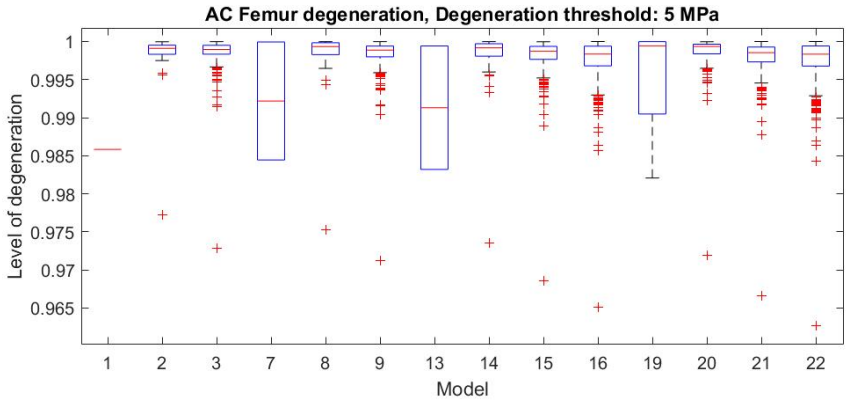

(b) The level of degeneration of the femoral AC.

Figure 3.2: The level of degeneration per model, computed with a degeneration threshold of 5 MPa

center, the unexpected degeneration at the locations of the outliers was assumed to be irregularities in the mesh. Therefore, the outliers were excluded from further data analysis. After correction of the outliers, 8 models showed at least one degenerated element on the AC of the tibia. The tibial AC of models 1, 2, 7, 8, 13, and 19 did not show any degeneration. For the femoral AC 13 models showed at least 1 degenerated element, only model 1 did not show any degeneration. Models 7 and 13 contained only 1 degenerated element. Analysis of differences in degeneration is limited by the lack of degeneration in multiple models. Therefore simulations were also run with a degeneration threshold of 3 MPa to better analyze the effect of altered Young's modulus on cartilage degeneration.

The distribution of the level of degeneration of all degenerated elements within each model after calculation with the degeneration threshold of 3 MPa was visualized in a boxplot for both the tibial and femoral AC in Figure 3.3. The data set shown was again corrected for outliers, which were the same elements as for the level of degeneration calculated with a degeneration threshold of 5 MPa. Models 1, 7, 13, and 19 did not show any degeneration on the tibial AC. On the AC femur, all models showed degeneration. The mean level of degeneration on the tibial AC was 0.9973 (sd: 0.0028) ranging from 1 (no degeneration) to 0.9812. The mean level of degeneration on the femoral AC was 0.9967 (sd: 0.0033) ranging from 1 to 0.9694.

3.3. Degenerated volume

The volume of the AC degeneration of the tibia and femur is presented for the completed models in Table 3.2 for both the calculation with a degeneration threshold of 5 MPa and 3 MPa. The volume of degeneration was 0 for multiple models with a degeneration threshold of 5 MPa. For sensitivity analysis purposes, the degenerated volumes calculated with a degeneration threshold of 3 MPa were used for further analyses and visualized in Appendix I. The degeneration showed similar patterns for

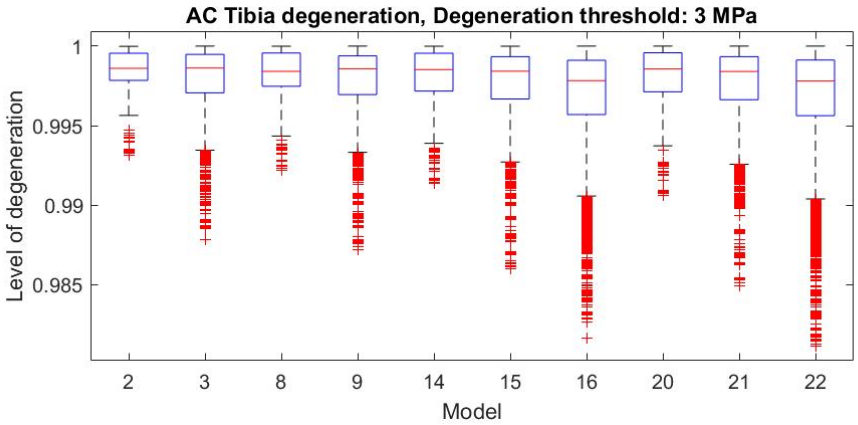

(a) The level of degeneration of the tibial AC.

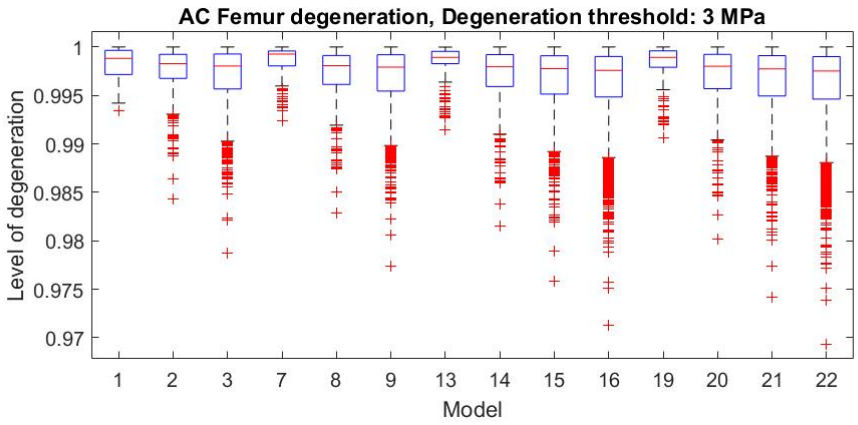

(b) The level of degeneration of the femoral AC.

Figure 3.3: The level of degeneration per model, computed with a degeneration threshold of 3 MPa

Model	Young's Modulus [MPa]		Degeneration threshold: 5MPa		Degeneration threshold: 3MPa	
	AC	Menisci	AC Tibia	AC Femur	AC Tibia	AC Femur
1	5	59	0	0	0	0.34
2	11	59	0	0.15	1.13	7.58
3	17	59	0.26	2.34	15.15	32.96
7	5	60	0	5.3e-4	0	0.77
8	11	60	0	0.30	1.41	9.12
9	17	60	0.375	2.92	1.41	9.12
13	5	73	0	5.3e-4	0	1.15
14	11	73	0.015	0.45	1.68	10.83
15	17	73	0.42	3.50	16.62	39.24
16	23	73	3.32	10.98	61.29	97.19
19	5	80	0	0.013	0	1.60
20	11	80	0.025	0.74	1.99	12.51
21	17	80	0.54	4.10	18.27	43.58
22	23	80	3.61	12.39	64.87	104.24

Table 3.2: Degenerated volume in mm^3.

	AC Tibia			AC Femur		
	a	b1	b2	a	b1	b2
Simple regression f(x1) = a*exp(b1*x1)	0.28 (0.15, 0.40)	0.24 (0.22, 0.26)		1.76 (1.06, 2.46)	0.18 (0.16, 0.20)	
Multiple regression f(x1,x2) = a*exp(b1*x1+b2*x2)	0.19 (0.062, 0.32)	0.23 (0.21, 0.25)	6.7e-3 (-2.7e-3, 0.016)	1.01 (0.32, 1.70)	0.17 (0.15, 0.19)	9.7e-3 (-2.1e-4, 0.02)

Table 3.3: The calculated equation coefficients with 95% confidence bounds for the simple and multiple regression.

all completed models, where degeneration appeared predominantly on the posterior half of the lateral AC.

In Figure 3.4 the volume of degeneration per model is presented in relation to the corresponding AC and meniscal Young's moduli for both the tibial and femoral AC. The mean volume of degeneration on the tibial AC was 14.19 mm^3 (sd: 21.94 mm^3), ranging from 0 mm^3 to 64.89 mm^3. The total volume of the tibial AC was 3714.93 mm^3. The mean volume of degeneration on the femoral AC was 28.40 mm^3 (sd: 34.30 mm^3), ranging from 0.34 mm^3 to 104.24 mm^3. The total volume of the femoral AC was 9849.93 mm^3.

The simple regression between the degenerated volume and the AC Young's modulus is shown in Figure 3.5. The calculated equation coefficients (with 95% confidence bounds) are presented in Table 3.3. The coefficient of determination for the regression with the tibial AC was R^2 = 0.994 (p<0.05). The coefficient of determination for the regression with the femoral AC was R^2 = 0.987 (p<0.05).

In the multiple regression analysis, the meniscal Young's modulus was added to the regression as a second independent variable. The AC Young's modulus was the first independent variable, x1. The meniscal Young's modulus was the second independent variable, x2. The calculated equation coefficients (with 95% confidence bounds) are presented in Table 3.3. The coefficient of determination for the multiple regression with the tibial AC was R^2 = 0.995 (p<0.05). The coefficient of determination for the regression with the femoral AC was R^2 = 0.989 (p<0.05).

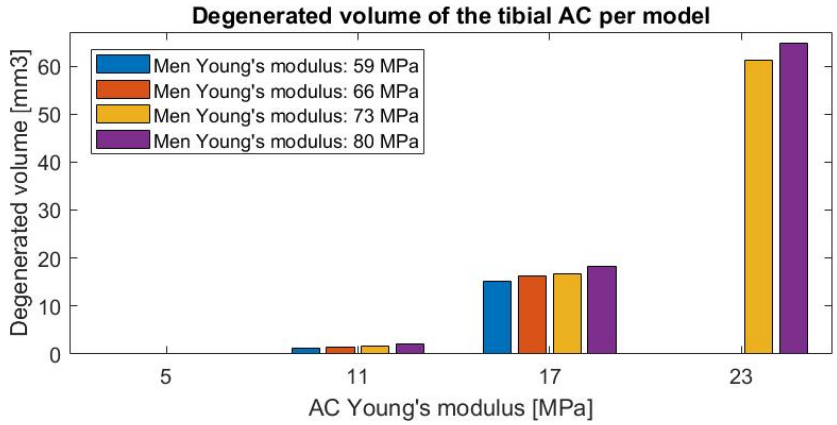

(a) Degenerated volume tibial AC.

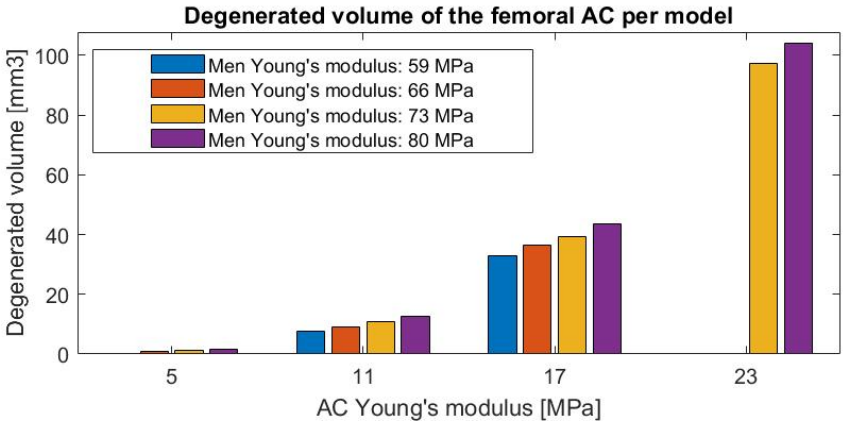

(b) Degenerated volume tibial AC.

Figure 3.4: Bar plot of the degenerated volume per model, per AC and meniscal Young's modulus, calculated with a degeneration threshold of 3 MPa.

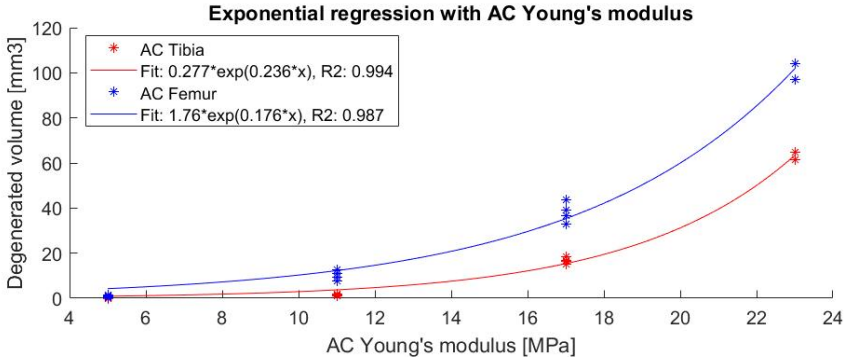

Figure 3.5: Simple regression of the degenerated volume with the AC Young's modulus as a single independent variable.

4

Discussion

The main objective of this thesis was to develop a patient-specific FE knee model of an ACLR patient. A degeneration algorithm was implemented in the model, to predict the development of cartilage degeneration. With this model, a sensitivity analysis was performed and a relation between the AC degenerated volume and AC Young's modulus was found. While this thesis only investigated the effect of altering the Young's moduli, a FE modeling workflow contains a larger number of parameters that can influence the workflow. Therefore, assumptions and choices made that influenced the computation time, complexity or outcome will be discussed prior to discussing the results.

First, segmentation of the knee bones and AC was performed manually, which is a time-consuming task. Segmentation of the AC was complicated due to the presence of disturbance artifacts from metallic attachments of the ACLR [50]. Due to the artifact, the segmented AC thickness might be affected. AC thickness influences the contact between the femur and tibia, as contact is made sooner if the AC is thicker. The segmentation was carefully performed and checked by an experienced radiologist, thus the potential inaccuracy in segmentation is expected to be limited, resulting in a minor influence on the outcome of the model. To speed up the time-consuming task of manual segmentation, automatic segmentation algorithms should be developed that account for the ACLR induced artifacts [51]. Human inspection of the segmentation would still be desired to verify the accuracy of the segmentation.

Second, the complexity of the geometries of the current model was an important factor in the decision for a tetrahedral mesh, as the computation of a hexahedral mesh for complex geometries is more time-consuming. Ramos and Simoes (2006) [52] performed a stress and strain test on the proximal femur with either a tetrahedral or hexahedral mesh, and concluded that the tetrahedral elements resulted in outcome values more closely to the experimental values. Whereas, the performance of hexahedral elements is less affected by mesh refinement as it has fewer convergence issues. Therefore it is recommended to further investigate hexahedral elements.

Third, the assembly of the current FE knee model contained the femur, tibia, their respective AC layers, both menisci and the collateral and cruciate ligaments. There is no consensus regarding the effect of the inclusion or exclusion of the patella. Where some studies show a change in internal-external rotation of the knee and increased reaction forces on the tibial AC [53], others found no effect on the kinematics and contact forces [36]. The patella was excluded to lower the complexity of the model and reduce the computational time.

Fourth, a multiscale workflow was used, where translational forces and the flexion-extension angle were derived from a musculoskeletal model with a one DoF knee [54]. This is a commonly used generic model for the extraction of forces, moments, and joint rotations based on patient-specific gait analysis [36, 55]. Compared to a 12 DoF knee model, using a 1 DoF model resulted in more excessive external rotation of the femur in the FE knee model at mid-stance. This was seen early in the midstance in the current FE knee model prior to locking the internal external rotation of the femur. This locking was done for stability purposes, even though increased external rotation following ACL injury has been reported [56]. Stability in the in-vivo knee is provided by the interaction between passive stabilizers; the ligaments and menisci, and active stabilizers; the muscles [57]. In-vivo, the menisci are connected to the tibia via meniscal horns with elastic behavior [58]. In literature, the meniscal horns have been modeled as springs with varying stiffnesses [59, 60]. Increased stiffness showed a decrease in AC con-

tact pressure error compared to experimental data [60]. As a large spring stiffness results in a minimal displacement of the meniscal horns, the meniscal horns of the current FE model were fully constrained for simplification. The rest of the menisci could still deform, providing stability and guiding the motion of the femur. Even though the menisci play a role in the stability, the ligaments were the primary knee-stabilizing components included in the model. In other words, the 4 linear springs were expected to stabilize the entire knee. In-vivo ligaments are more complex than a single linear spring with 1 line of action. The cruciate ligaments are both composed of 2 bundles; the anteromedial and posterolateral bundles for the ACL, and the anterolateral and posteromedial bundles for the PCL [61]. The LCL, and MCL both have different bundles and sections as well. The bundles within the ligaments differ in size and attachment site, resulting in different lines-of-action, and unique functions of the bundles [62]. Therefore, Blankevoort (1991) suggested modeling the knee ligaments as multiple non-linear springs [63]. Adding springs to the current FE knee model adds complexity and introduces new parameters to optimize such as attachment sites, lines-of-action, stiffnesses, and pre-strain. Numerous simulations with multiple springs were tested, but convergence issues remained when the femur was free to move in all DoFs. The expectation is that successful modeling of the multiple springs requires a combination of multiple of the parameters mentioned. Due to project time constraints, the multiple springs were not successfully implemented in the FE knee model of the current thesis. Therefore, stability was provided to the model by locking the medial-lateral translation, and the internal-external rotation. Opening up the medial-lateral translation, and the internal-external rotation was expected to mostly influence the shear stress, while the degeneration algorithm implemented in this thesis was based on the max principal stress. In terms of kinematics, the opening of the DoFs is expected to have consequences, but in terms of the expected max principal stress, the effect is expected to be smaller, and thus also the effects on the level of degeneration are expected to be relatively small. However, when locking DoFs, the physiological kinematic behavior of the knee joint is compromised and the real-world representability of the model is reduced. Therefore, optimization of ligament modeling should be further researched and implemented.

Fifth, the interaction definitions were defined as a node-to-surface contact discretization. The node-to-surface contact was selected over the surface-to-surface contact, due to the large fraction of the model that was involved in the contact. Using surface-to-surface discretization can largely increase solution time. Furthermore, the assignment of the master and slave surfaces in the interaction definitions influences the way the contact behaves, and how stresses are transmitted between surfaces. The main rule for the assignment is that the larger surface part should be the master surface. Master nodes on the master surface are able to penetrate the slave surface, whereas slave nodes cannot penetrate the master surface. Therefore, the slave surface should have a finer mesh than the master surface to limit penetration. Lastly, the master surface should be the body with higher material stiffness. The femoral AC was assigned to be the master surface in all the involved contact pairs, as it was a significantly larger body and had a coarser mesh size compared to the AC tibia and the menisci. However, the menisci were assigned a higher Young's modulus in all models included in the sensitivity analysis. A slave surface with a higher stiffness compared to the master surface could affect the transfer of stresses between the surfaces.

Sixth, the degeneration algorithm in the current thesis was based solely on max principal stresses while other mechanisms such as proteoglycan depletion are thought to contribute to AC degeneration as well [64]. Mononen et al (2018) included a proteoglycan depletion algorithm in one of their studies [65]. The AC degeneration and proteoglycan depletion were both independent processes, as the proteoglycan depletion was calculated based on principal shear strains. In a follow-up study, they excluded the proteoglycan depletion in the algorithm [10]. As the first sign of OA in AC is collagen fibrillation, combined with the consideration of simulation time, these considerations led to the inclusion of only the max principal stress as a factor for AC degeneration [41]. Furthermore, only one iteration was performed as this was assumed to predict 70% of the degeneration that would occur over 5 years [10]. Over the course of 5 years, factors such as weight, kinematics, physical activity, and health-related aspects can change. These changes are not accounted for in the current model. This should be kept in mind when interpreting the level of degeneration calculated by the algorithm.

Based on these implemented assumptions, the AC degeneration was calculated. The level of degeneration calculated with the current FE model showed minimal to no degeneration with a degeneration threshold of 5 MPa. To validate these findings, a 5-year follow-up MRI of the same patient was

evaluated by clinicians. Based on the follow-up MRI it was confirmed that the patient did not show any tibiofemoral cartilage degeneration at 5 years. Even when decreasing the degeneration threshold to 3 MPa, the calculated AC degeneration was small. The largest degeneration was 0.9812 on the AC tibia and 0.9694 on the AC femur. These levels of degeneration indicate minimal collagen fibrillation, which might even be present in the AC of people experiencing no joint pain or visible OA [66, 67]. However, the regions where minor degeneration was calculated, could be indications of vulnerability to more degeneration in the future. In terms of the statistical analysis, these small levels of degeneration limited the ability to show differences between the models with varying Young's moduli. Therefore, the volume of degeneration AC was selected as the dependent variable for the statistical analysis. The range of degenerated volumes of 0 mm^3 to 104.24 mm^3 was within a similar range as found by Mononen et al. (2019), of 0 mm^3 to approximately 140 mm^3 [10]. The subjects included in their study did not have ACLR but were confirmed to develop varying levels of OA at the 4-year follow-up.

For both the tibial and femoral AC, the standard deviation of the degenerated volume was larger than the mean degenerated volume. As a negative value of the degenerated volume is not possible, the larger standard deviation suggests that the data was heavily tailed. This can be seen in the bar plots in Figure 3.4, where the degenerated volume increases with increasing AC Young's modulus. The degenerated volume seems to increase minimally with increasing meniscal Young's modulus. The simple regression with AC Young's modulus as an independent variable resulted in a significant coefficient of determination for both AC (R2: 0.994, $p<0.05$ and R2: 0.989, $p<0.05$, for tibia and femur respectively), indicating strong predictability of the degenerated volume based on the AC Young's modulus for both AC. To evaluate the relative effect of the AC and meniscal Young's moduli on the degenerated volume, multiple regression was performed. For both AC, the coefficient of determination was not affected when the meniscal Young's modulus was added to the regression. Thus, the meniscal Young's modulus did not significantly affect the degenerated volume.

The sample size of 14 models and only 4 different AC and meniscal Young's moduli should be considered. A smaller data set is easier to fit with high accuracy due to limited data points. Notably, the degenerated volume has a maximum value it can reach. This maximum is determined by the maximum area of contact between the tibial and femoral AC during the gait cycle. This maximum was not included in the regression equation. The exponential equation implied that a difference between lower values of Young's moduli had a smaller effect on the degenerated volume, compared to the same difference in value of larger Young's moduli. As opposed to a linear relation, where the increase in degenerated volume would have been the same for a certain difference in Young's modulus.

Young's modulus is a measure of the ability of a material to withstand deformation under a given load [68]. As the max principal stress is determined by the applied load it would not directly be affected by Young's modulus, but an indirect effect was detected. The Young's modulus affected the stiffness of AC and the level of deformation it experienced. An increase or decrease in deformation altered the stress distribution within the AC. These effects were demonstrated by the differences in peak max principal stresses between the models. Under the same load, models with higher AC Young's moduli showed higher peak max principal stresses. The higher stiffness of the material resulted in a larger distributed area of the stress due to decreased tendency for deformation. This explained the increased degenerated volume calculated for models with higher AC Young's moduli.

The peak max principal stress calculated for the current FE ACLR knee model ranged between 2.84 MPa and 21.82 MPa. These values were in the same ranges as found in other FE ACLR knee models (3.36 MPa - 12.57 MPa [11, 35]). The shift in the location of the max principal stress, as seen in Figure 3.1, was also presented in literature. A higher max principal stress on the lateral condyle was found in patients with ACLR [69]. Even though a similar shift was seen in literature [6], the locked DoF potentially affected the shift as well. As the medial-lateral translation and the internal-external rotation were locked, forces acting in these directions were translated into other DoF. Since medial-lateral translation is locked, a force working in this direction might result in a varus-valgus moment, dependent on the distance to the center of rotation. According to clinician analysis of the patient-specific follow-up data, a small valgus of 0.7°from fully straight was detected. Furthermore, the lateral tibial AC compartment of the patient was thicker compared to the medial compartment. This is in line with literature, where the AC on the lateral compartment is reported to be generally thicker and contains a more centered region of maximum thickness compared to the medial side where the thickness is more equally distributed [70]. The centered peak thickness on the lateral compartment makes this compartment more vulnerable to the combination of kinematic changes and a minor valgus. It has

been reported that kinematic changes as a consequence of ACL injuries can displace the location of repetitive contact during gait to unconditioned AC regions [7]. Together with a minor valgus which can increase contact stress on the lateral compartment, the peak stresses on both AC can increase and displace to AC regions that are not conditioned for these peak stresses [70].

The peak max principal stress on the AC tibia occurred between 0.11 sec and 0.12 sec for all models. The models that failed to converge all aborted between 0.10 sec and 0.11 sec. As the AC and meniscal Young's moduli were the only parameters that changed, the inability of the current FE model to converge to a solution is most likely related to the Young's moduli. It was observed that the model with an AC Young's modulus of 23 MPa did not converge when combined with a meniscal Young's Modulus of 59 MPa or 66 MPa. The models with an AC Young's modulus of 23 MPa and a meniscal Young's modulus of 73 MPa or 80 MPa did manage to converge. The Young's modulus of the AC is highly patient-specific, with factors such as age, physical activity, and overall health, playing a substantial role in the stiffness of the AC [71, 72]. The higher Young's moduli used for AC modeling in literature [12], however, might not be physiologically accurate [73]. The type of errors documented by Abaqus were max penetration errors, where the nodes causing the error varied per model. The nodes that caused errors were often part of the contact pair between the medial meniscus and one of the AC. None of the errors arose from AC - AC contact. The master and slave surface assignments could play a role in the errors, as this affected the penetration allowed between contacting surfaces. Nodes on the slave surface are allowed to penetrate the master surface up to a penetration tolerance of 0.1% of the length between 2 nodes on the master surface. If the penetration is larger than the penetration tolerance, the contact stiffness is locally augmented and a new iteration is attempted. For the failed models, the penetration errors could not be solved within the maximum number of iteration attempts allowed. Possible solutions include improvement of the mesh or adjustment of the contact behavior. The mesh can be improved by decreasing mesh size, upgrading the tetrahedral element to have more nodes (tet10), or applying a hexahedral mesh. Contact behavior can be adjusted by allowing more penetration, reassigning the master and slave surfaces, or assigning other contact formulations.

Even though the max principal stresses and levels of degeneration calculated were within expected ranges, recommendations for improvements of the workflow were presented. The effect of implementing these recommendations on simulation times should be considered. For the current workflow, the simulation time of the completed models took approximately 20 hours. Simulation times of 21 hours [34] up to 4 days [36] have been reported for FE knee models of similar complexity in terms of included segments.

The current thesis was a setup for a proof-of-concept to establish a workflow for a patient-specific FE knee model with an implemented degeneration algorithm. Through a multiscale modeling workflow, patient-specific MRI and gait-analysis data were converted into a FE knee model, which determines the AC degeneration levels based on the max principal stresses. A foundation was made for further development of the model towards a clinically applicable model, guided by the indicated future recommendations for improvements of the workflow made at the beginning of the discussion. The performed sensitivity analysis shows the importance of parameter consideration. A sensitivity analysis was performed solely based on changes in the Young's moduli but did already show how the uncertainty in a single parameter can affect the models' outcome.

5 Conclusion

The multiscale FE workflow presented in this thesis has proven to be a promising approach for the estimation of AC degeneration occurring in ACLR knees. The exponential relation between the AC Young's modulus and the degenerated volume indicated that uncertainties in these values lead to differences in the calculated degenerated volume. These differences suggest that a generic AC Young's modulus based on literature might not be appropriate for a patient-specific FE ACLR knee model. There is a need for better estimations of patient-specific AC Young's moduli. The workflow did not show a sensitivity to the meniscal Young's modulus, indicating that the use of a generic meniscal Young's modulus is sufficient.

The established FE workflow provides a foundation for future research studies. The predictability of AC degeneration with the model should be researched by including a larger group of ACLR patients, preferably including patients who show AC degeneration at the follow-up MRI. Furthermore, the current model implemented single linear springs, and the medial-lateral translation and internal-external rotation of the femur were locked. In future studies, modeling techniques of the ligaments should be researched to improve the physiological behavior of the modeled ligaments and allow for the opening of all DoF. The effect of implementing these changes on the calculated degeneration should be assessed, as well as the increase in simulation time due to higher model complexity.

In conclusion, the proposed workflow showed sufficient promise to continue research of this FE ACLR knee modeling workflow and its ability to predict AC degeneration.

Bibliography

[1] W. Montagna, Albert M. K., and Carlisle K. S. *Atlas of Normal Human Skin*. Electronic Book. 1992.

[2] A. J. Sophia Fox, A. Bedi, and S. A. Rodeo. “The basic science of articular cartilage: structure, composition, and function”. In: *Sports Health* 1.6 (2009), pp. 461–8.

[3] A. Cui et al. “Global, regional prevalence, incidence and risk factors of knee osteoarthritis in population-based studies”. In: *EClinicalMedicine* 29-30 (2020), p. 100587.

[4] D. Prieto-Alhambra et al. “Incidence and risk factors for clinically diagnosed knee, hip and hand osteoarthritis: influences of age, gender and osteoarthritis affecting other joints”. In: *Ann Rheum Dis* 73.9 (2014), pp. 1659–64.

[5] A. G. Culvenor et al. “Early knee osteoarthritis is evident one year following anterior cruciate ligament reconstruction: a magnetic resonance imaging evaluation”. In: *Arthritis Rheumatol* 67.4 (2015), pp. 946–55.

[6] S. Van Rossom et al. “Knee cartilage thickness, T1ρ and T2 relaxation time are related to articular cartilage loading in healthy adults”. In: *PLoS One* 12.1 (2017).

[7] K. Marriott et al. “Five-year changes in gait biomechanics after concomitant high tibial osteotomy and ACL reconstruction in patients with medial knee osteoarthritis”. In: *Am J Sports Med* 43.9 (2015), pp. 2277–85. ISSN: 0363-5465.

[8] Z. Trad, A. Barkaoui, and M. Chafra. “A three dimensional finite element analysis of mechanical stresses in the human knee joint: Problem of cartilage destruction”. In: *Journal of Biomimetics, Biomaterials and Biomedical Engineering* 32 (2017), pp. 29–39.

[9] R. Mootanah et al. “Development and validation of a computational model of the knee joint for the evaluation of surgical treatments for osteoarthritis”. In: *Computer Methods in Biomechanics and Biomedical Engineering* 17.13 (2014), pp. 1502–1517.

[10] M. E. Mononen, M. K. Liukkonen, and R. K. Korhonen. “Utilizing Atlas-Based Modeling to Predict Knee Joint Cartilage Degeneration: Data from the Osteoarthritis Initiative”. In: *Annals of Biomedical Engineering* 47.3 (2019), pp. 813–825.

[11] P. O. Bolcos et al. “Subject-specific biomechanical analysis to estimate locations susceptible to osteoarthritis—Finite element modeling and MRI follow-up of ACL reconstructed patients”. In: *Journal of Orthopaedic Research* (2021).

[12] E. C. Meyer and R. C. Haut. “Biomechanical response of the knee in sports injury scenarios”. In: *The Knee: Current Concepts in Kinematics, Injury Types, and Treatment Options*. 2012, pp. 1–65.

[13] G. A. Orozco et al. “Prediction of local fixed charge density loss in cartilage following ACL injury and reconstruction: A computational proof-of-concept study with MRI follow-up”. In: *Journal of Orthopaedic Research* 39.5 (2021), pp. 1064–1081. ISSN: 0736-0266.

[14] R. Huang, H. Zheng, and Q. Xu. “Biomechanical evaluation of different techniques in double bundle anterior cruciate ligament reconstruction using finite element analysis”. In: *Journal of Biomimetics, Biomaterials, and Tissue Engineering* 13.1 (2012), pp. 55–68.

[15] A. H. Alafiah, M. Normahira, and M. N. Anas. “A three dimensional finite element of anterior cruciate ligament model”. In: *Advanced Materials Research*. Vol. 626. 2013, pp. 896–901.

[16] A. Vulović, N. Filipović, and B. Ristić. “Effects of ruptured anterior cruciate ligament and medial meniscectomy on stress distribution of human knee joint at full extension”. In: *2015 IEEE 15th International Conference on Bioinformatics and Bioengineering, BIBE 2015*. 2015.

[17] M. Smith. *ABAQUS/Standard User’s Manual, Version 6.9*. English. United States: Dassault Systèmes Simulia Corp, 2009.

[18] J. N. Reddy. *Introduction to the finite element method*. McGraw-Hill Education, 2019. ISBN: 1259861902.

[19] A. Paz et al. “Expediting finite element analyses for subject□specific studies of knee osteoarthritis: A literature review”. In: *Applied Sciences (Switzerland)* 11.23 (2021). ISSN: 20763417 (ISSN).

[20] A. G. Culvenor et al. “Rehabilitation after anterior cruciate ligament and meniscal injuries: a best-evidence synthesis of systematic reviews for the OPTIKNEE consensus”. In: *Br J Sports Med* 56.24 (2022), pp. 1445–1453. ISSN: 0306-3674 (Print) 0306-3674.

[21] E. M. Macri et al. “Does patellar alignment or trochlear morphology predict worsening of patellofemoral disease within the first 5 years after anterior cruciate ligament reconstruction?” In: *Eur J Radiol* 113 (2019), pp. 32–38.

[22] P. Sritharan et al. “Between-Limb Differences in Patellofemoral Joint Forces During Running at 12 to 24 Months After Unilateral Anterior Cruciate Ligament Reconstruction”. In: *Am J Sports Med* 48.7 (2020), pp. 1711–1719. ISSN: 1552-3365 (Electronic) 0363-5465 (Linking).

[23] P. Sritharan et al. “Patellofemoral and tibiofemoral joint loading during a single-leg forward hop following ACL reconstruction”. In: *J Orthop Res* 40.1 (2022), pp. 159–169. ISSN: 1554-527X (Electronic) 0736-0266 (Linking).

[24] J. VanMeter. “Basics of Magnetic Resonance Imaging”. In: (2008).

[25] W. C. Peh et al. “The effect of using shorter echo times in MR imaging of knee menisci: a study using a porcine model”. In: *AJR Am J Roentgenol* 172.2 (1999), pp. 485–8. ISSN: 0361-803X (Print) 0361-803x.

[26] Slicer Community. Web Page. 2020. URL: `https://www.slicer.org/`.

[27] A. Fedorov et al. “3D Slicer as an image computing platform for the Quantitative Imaging Network”. In: *Magn Reson Imaging* 30.9 (2012), pp. 1323–41.

[28] A. Lassoan. *3D Slicer segmentation Recipes*. Web Page. URL: `https://lassoan.github.io/SlicerSegmentationRecipes/ObliqueSliceSegmentation/`.

[29] C. S. Pinter, A. Lasso, and Fichtinger G. “Polymorph segmentation representation for medical image computing”. In: *Computer Methods and Programs in Biomedicine* 171 (2019), pp. 19–26.

[30] S. L. Delp et al. “OpenSim: Open-Source Software to Create and Analyze Dynamic Simulations Of Movement.” In: *IEEE Transactions on Biomedical Engineering* (2007).

[31] E. M. Arnold et al. “A model of the lower limb for analysis of human movement”. In: *Ann Biomed Eng* 38.2 (2010), pp. 269–79.

[32] A. D. Sylvester, S. G. Lautzenheiser, and P. A. Kramer. “A review of musculoskeletal modelling of human locomotion”. In: *Interface Focus* 11.5 (2021), p. 20200060. ISSN: 2042-8898 (Print) 2042-8901 (Electronic) 2042-8898 (Linking).

[33] T. P. Andriacchi et al. “Rotational changes at the knee after ACL injury cause cartilage thinning”. In: *Clinical Orthopaedics and Related Research* 442 (2006), pp. 39–44.

[34] R. W. Westermann, B. R. Wolf, and J. M. Elkins. “Effect of ACL reconstruction graft size on simulated Lachman testing: a finite element analysis”. In: *The Iowa orthopaedic journal* 33 (2013), pp. 70–77.

[35] K. S. Halonen et al. “Optimal graft stiffness and pre-strain restore normal joint motion and cartilage responses in ACL reconstructed knee”. In: *Journal of Biomechanics* 49.13 (2016), pp. 2566–2576.

[36] P. O. Bolcos et al. “Comparison between kinetic and kinetic-kinematic driven knee joint finite element models”. In: *Sci Rep* 8.1 (2018), p. 17351.

[37] C. Wan, Z. Hao, and S. Wen. “The finite element analysis of three grafts in the anterior cruciate ligament reconstruction”. In: *Proceedings - 2011 4th International Conference on Biomedical Engineering and Informatics, BMEI 2011*. Vol. 3, pp. 1338–1342.

[38] L. X. Wang et al. “Anterior cruciate ligament reconstruction and cartilage contact forces-A 3D computational simulation”. In: *Clinical Biomechanics* 30.10 (2015), pp. 1175–1180. ISSN: 0268-0033.

[39] D. J. Benson and J. O. Hallquist. “A single surface contact algorithm for the post-buckling analysis of shell structures”. In: *Computer methods in applied mechanics and engineering* 78.2 (1990), pp. 141–163.

[40] M. E. Mononen et al. “A novel method to simulate the progression of collagen degeneration of cartilage in the knee: Data from the osteoarthritis initiative”. In: *Scientific Reports* 6 (2016).

[41] M. K. Liukkonen et al. “Simulation of Subject-Specific Progression of Knee Osteoarthritis and Comparison to Experimental Follow-up Data: Data from the Osteoarthritis Initiative”. In: *Sci Rep* 7.1 (2017), p. 9177. ISSN: 2045-2322.

[42] B. B. Seedhom. “Conditioning of cartilage during normal activities is an important factor in the development of osteoarthritis”. In: *Rheumatology* 45.2 (Nov. 2005), pp. 146–149. ISSN: 1462-0324.

[43] E. K. Danso et al. “Comparison of nonlinear mechanical properties of bovine articular cartilage and meniscus”. In: *J Biomech* 47.1 (2014), pp. 200–6. ISSN: 0021-9290.

[44] Delft High Performance Computing Centre (DHPC). *DelftBlue Supercomputer (Phase 1)*. `https://www.tudelft.nl/dhpc/ark:/44463/DelftBluePhase1`. 2022.

[45] T. Brooks, M. Garnich, and M. Jermy. “Sensitivity of material model parameters on finite element models of infant head impacts”. In: *Biomechanics and modeling in mechanobiology* 20.5 (2021), pp. 1675–1688.

[46] N. B. Rooks, T. F. Besier, and M. T. Y. Schneider. “A Parameter Sensitivity Analysis on Multiple Finite Element Knee Joint Models”. In: *Frontiers in Bioengineering and Biotechnology* 10 (2022), pp. 841–882.

[47] D. D. Jebaseelan et al. “Sensitivity studies of pediatric material properties on juvenile lumbar spine responses using finite element analysis”. In: *Medical & biological engineering & computing* 50 (2012), pp. 515–522.

[48] S. Kumaresan, N. Yoganandan, and F. A. Pintar. “Finite element analysis of the cervical spine: a material property sensitivity study”. In: *Clinical biomechanics* 14.1 (1999), pp. 41–53.

[49] G. James et al. *An introduction to statistical learning*. Vol. 112. Springer, 2013.

[50] A. Grassi et al. “Magnetic resonance imaging after anterior cruciate ligament reconstruction: a practical guide”. In: *World journal of orthopedics* 7.10 (2016), p. 638.

[51] M. Perslev et al. “Cross-cohort automatic knee MRI segmentation with multi-planar U-nets”. In: *Journal of Magnetic Resonance Imaging* 55.6 (2022), pp. 1650–1663.

[52] A. Ramos and J. A. Simoes. “Tetrahedral versus hexahedral finite elements in numerical modelling of the proximal femur”. In: *Med Eng Phys* 28.9 (2006), pp. 916–24. ISSN: 1350-4533 (Print) 1350-4533 (Linking).

[53] K. S. Halonen et al. “Importance of Patella, Quadriceps Forces, and Depthwise Cartilage Structure on Knee Joint Motion and Cartilage Response During Gait”. In: *Journal of Biomechanical Engineering* 138.7 (2016). ISSN: 0148-0731 1528-8951.

[54] S. Ramezani et al. “Validation of Musculoskeletal Models Using Single Degree of Freedom Analysis”. In: ResearchGate, 2020.

[55] E. M. Arnold et al. “A model of the lower limb for analysis of human movement”. In: *Ann Biomed Eng* 38.2 (2010), pp. 269–79. ISSN: 0090-6964 (Print) 0090-6964.

[56] Y. Zhang et al. “Anterior Cruciate Ligament Injuries Alter the Kinematics of Knees With or Without Meniscal Deficiency”. In: *Am J Sports Med* 44.12 (2016), pp. 3132–3139. ISSN: 1552-3365 (Electronic) 0363-5465 (Linking).

[57] O. D. Schipplein and T. P. Andriacchi. “Interaction between active and passive knee stabilizers during level walking”. In: *J Orthop Res* 9.1 (1991), pp. 113–9. ISSN: 0736-0266 (Print) 0736-0266 (Linking).

[58] D. F. Villegas et al. “Failure properties and strain distribution analysis of meniscal attachments”. In: *Journal of Biomechanics* 40.12 (2007), pp. 2655–2662. ISSN: 0021-9290.

[59] J. Yao et al. “Sensitivities of medial meniscal motion and deformation to material properties of articular cartilage, meniscus and meniscal attachments using design of experiments methods”. In: (2006).

[60] T. L. Haut Donahue et al. “How the stiffness of meniscal attachments and meniscal material properties affect tibio-femoral contact pressure computed using a validated finite element model of the human knee joint”. In: *Journal of Biomechanics* 36.1 (2003), pp. 19–34. ISSN: 0021-9290.

[61] J. D. Hassebrock et al. “Knee Ligament Anatomy and Biomechanics”. In: *Sports Medicine and Arthroscopy Review* 28(3) (2020), pp. 80–86.

[62] Hamid Naghibi B. et al. “The influence of ligament modelling strategies on the predictive capability of finite element models of the human knee joint”. In: *Journal of Biomechanics* 65 (2017), pp. 1–11.

[63] L. Blankevoort and R. Huiskes. “Ligament-bone interaction in a three-dimensional model of the knee”. In: *J Biomech Eng* 113.3 (1991), pp. 263–9. ISSN: 0148-0731 (Print) 0148-0731.

[64] G. A. Orozco et al. “A novel mechanobiological model can predict how physiologically relevant dynamic loading causes proteoglycan loss in mechanically injured articular cartilage”. In: *Sci Rep* 8.1 (2018), p. 15599. ISSN: 2045-2322.

[65] M. E. Mononen et al. “New algorithm for simulation of proteoglycan loss and collagen degeneration in the knee joint: Data from the osteoarthritis initiative”. In: *J Orthop Res* 36.6 (2018), pp. 1673–1683. ISSN: 0736-0266.

[66] J. A. Martin and J. A. Buckwalter. “Roles of articular cartilage aging and chondrocyte senescence in the pathogenesis of osteoarthritis”. In: *The Iowa orthopaedic journal* 21 (2001), p. 1.

[67] W. W. Curl et al. “Cartilage injuries: a review of 31,516 knee arthroscopies”. In: *Arthroscopy: The Journal of Arthroscopic & Related Surgery* 13.4 (1997), pp. 456–460.

[68] The Editors of Encyclopedia Britannica. *Young’s Modulus*. Encyclopedia Brittanica, 2023.

[69] P. O. Bolcos et al. “Identification of locations susceptible to osteoarthritis in patients with anterior cruciate ligament reconstruction: Combining knee joint computational modelling with follow-up T-1 rho and T-2 imaging”. In: *Clinical Biomechanics* 79 (2020). ISSN: 0268-0033.

[70] T. P. Andriacchi. “Valgus alignment and lateral compartment knee osteoarthritis: a biomechanical paradox or new insight into knee osteoarthritis?” In: *Arthritis Rheum* 65.2 (2013), pp. 310–3. ISSN: 1529-0131 (Electronic) 0004-3591 (Print) 0004-3591 (Linking).

[71] M. Hudelmaier et al. “Age-related changes in the morphology and deformational behavior of knee joint cartilage”. In: *Arthritis & Rheumatism* 44.11 (2001), pp. 2556–2561.

[72] F. Eckstein et al. “In vivo cartilage deformation after different types of activity and its dependence on physical training status”. In: *Annals of the rheumatic diseases* 64.2 (2005), pp. 291–295.

[73] J S Jurvelin, M D Buschmann, and E B Hunziker. “Mechanical anisotropy of the human knee articular cartilage in compression”. In: *Proceedings of the Institution of Mechanical Engineers, Part H: Journal of Engineering in Medicine* 217.3 (2003), pp. 215–219.

A

Appendix: Workflow FE model

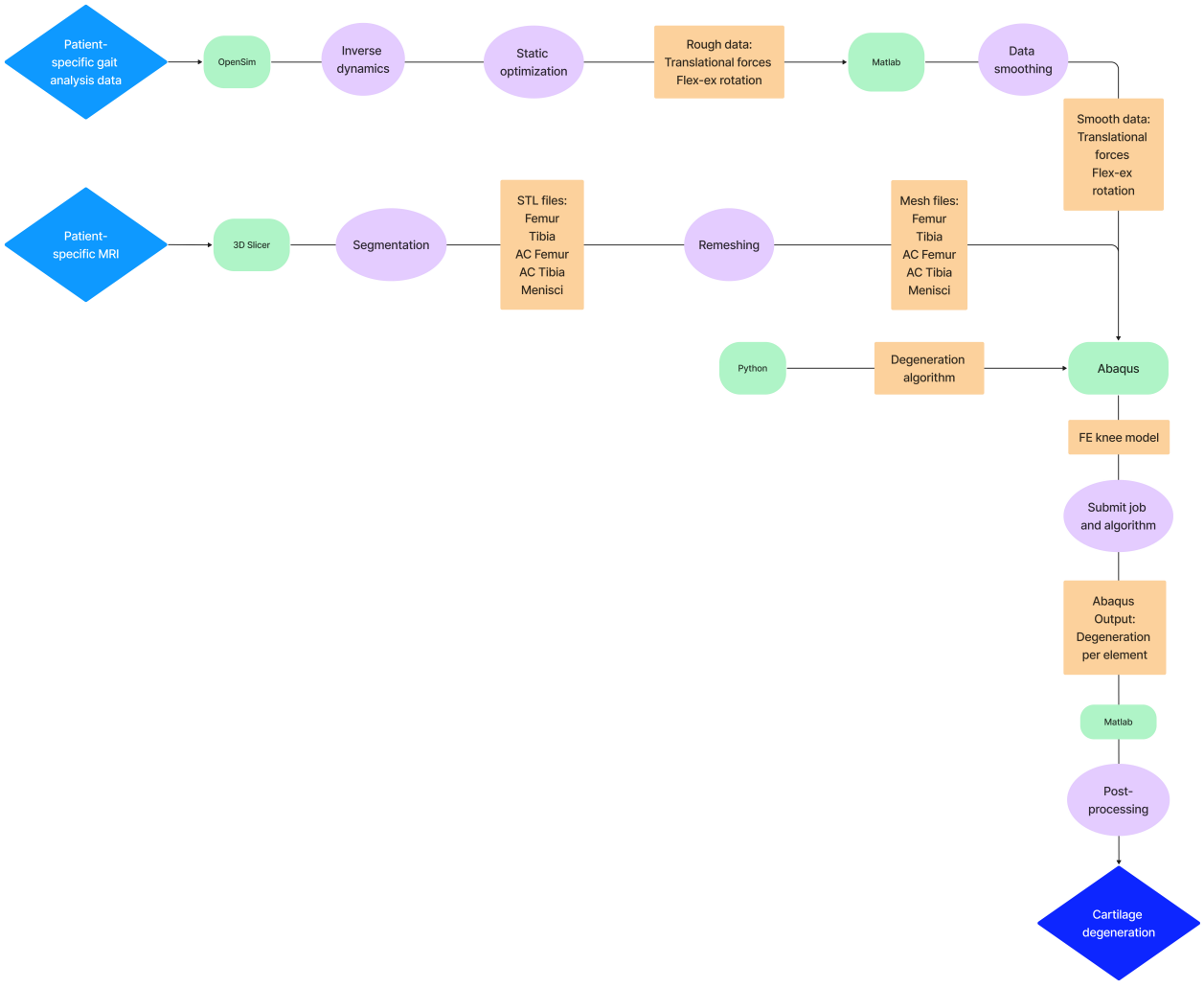

Figure A.1: A global representation of the established FE workflow. The main patient-specific input parameters are knee MRI and gait analysis data, which are implemented in the workflow to create a patient-specific FE knee model with the aim of estimating cartilage degeneration, the main output parameter of the workflow.

B

Appendix: Gait data smoothing code

```
%% Load data
Data = readtable('Gait_data.xlsx');
time = table2array(Data(:,1));
Time = time- time(1); % time starting from 0
fx_force = table2array(Data(:,2)); % Anterior - posterior force
fy_force = table2array(Data(:,3)); % Distal - proximal force
fz_force = table2array(Data(:,4)); % Medial - lateral force
Knee_angle = table2array(Data(:,5)); % Flexion - extension rotation

%% Select stance phase
stance_phase = find(time<2.067); % time point manually observed in OpenSim
stance_time = time(stance_phase);

fx_stance = fx_force(stance_phase);
fy_stance = fy_force(stance_phase);
fz_stance = fz_force(stance_phase);
Angle_stance = Knee_angle(stance_phase);

%% Smoothen data
fx_smooth_start = smoothdata(fx_stance,'gaussian',15);
fx_smooth_end = smoothdata(fx_stance,'gaussian',5);
fx_smooth = [fx_smooth_start(1:19);fx_smooth_end(20:end)];

fy_smooth_start = smoothdata(fy_stance,'gaussian',15);
fy_smooth_end = smoothdata(fy_stance,'gaussian',5);
fy_smooth = [fy_smooth_start(1:9);fy_smooth_end(10:end)];

fz_smooth_start = smoothdata(fz_stance,'gaussian',15);
fz_smooth_end = smoothdata(fz_stance,'gaussian',5);
fz_smooth = [fz_smooth_start(1:9);fz_smooth_end(10:end)];

Angle_smooth = smoothdata(Angle_stance,'gaussian',3);

% Plot the data to check the smoothening
figure(9)
plot(stance_time,fx_smooth,'--', stance_time,fx_stance,'LineWidth',1)
legend('Filtered data','rough data')
title('Fx force during stance phase')
xlabel('Time [s]')
```

```
ylabel('Force [N]')

figure(10)
plot(stance_time,fy_smooth,'--', stance_time,fy_stance,'LineWidth',1)
legend('Filtered data','rough data')
title('Fy force during stance phase')
xlabel('Time [s]')
ylabel('Force [N]')

figure(11)
plot(stance_time,fz_smooth,'--', stance_time,fz_stance,'LineWidth',1)
legend('Filtered data','rough data')
title('Fz force during stance phase')
xlabel('Time [s]')
ylabel('Force [N]')

figure(12)
plot(stance_time,Angle_smooth,'--', stance_time,Angle_stance,'LineWidth',1)
legend('Filtered data','rough data')
title('Flex-ext rotation')
xlabel('Time [s]')
ylabel('Angle [deg]')

%% Write data to excel sheets
Time_per = stance_time - stance_time(1); % Have the time period start at 0
xlswrite('Filtered_data.xls',{'Time'},1,'A1');
xlswrite('Filtered_data.xls',Time_per,1,'A2');
xlswrite('Filtered_data.xls',{'fx'},1,'B1');
xlswrite('Filtered_data.xls',fx_smooth,1,'B2');
xlswrite('Filtered_data.xls',{'fy'},1,'C1');
xlswrite('Filtered_data.xls',fy_smooth,1,'C2');
xlswrite('Filtered_data.xls',{'fz'},1,'D1');
xlswrite('Filtered_data.xls',fz_smooth,1,'D2');
xlswrite('Filtered_data.xls',{'Angle deg'},1,'F1');
xlswrite('Filtered_data.xls',Angle_smooth,1,'F2');
```

C

Appendix: Transformation matrix

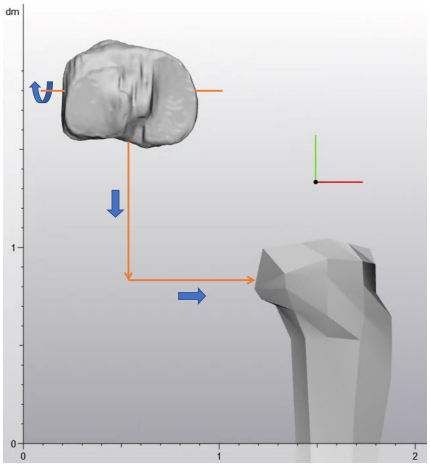

(a) Original misalignment of the tibial parts of the OpenSim body and 3D-slicer segment. The reference coordinate systems align, but the tibial parts do not.

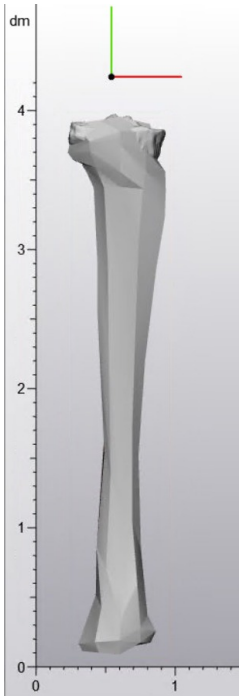

(b) Alignment of the tibial heads.

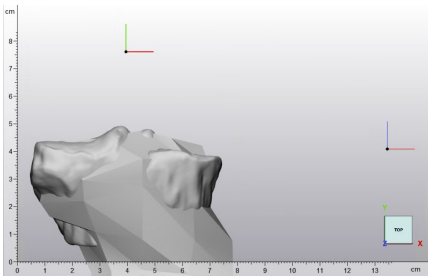

(c) Alignment of the tibial heads, with a visualization of the misalignment of the reference frames.

Translations	X	Y	Z
Trial 1	-99.0000	40.1993	35.3842
Trial 2	-95.0000	45.3581	35.3914
Trial 3	-95.0000	45.3731	33.4019
Mean	-96.33333	43.84343	34.72583

Rotations	X	Y	Z
1	90.1698	0	0
2	89.9084	0	0
3	90.1698	0	0
Mean	90.0827	0	0

Table C.1: The transformation matrix, with the translations in mm and the rotations in degree.

D

Appendix: Mesh Convergence study

Sweep layer		AC femur	AC tibia	Lateral meniscus	Medial meniscus
2	Edge length	0.2	0.4	0.4	0.3
	# of elements	79508	31332	7681	19712
3	Edge length	0.35	0.3	0.3	0.2
	# of elements	106019	58062	14206	45828
4	Edge length	0.3	0.2	0.25	0.175
	# of elements	147294	134474	20794	60328
5	Edge length	0.25	0.2	0.2	0.125
	# of elements	215009	134474	33150	120184
6	Edge length	0.2	0.2	0.175	0.1
	# of elements	340666	134474	43694	188888

Table D.1: Mesh parameters used in the mesh convergence study

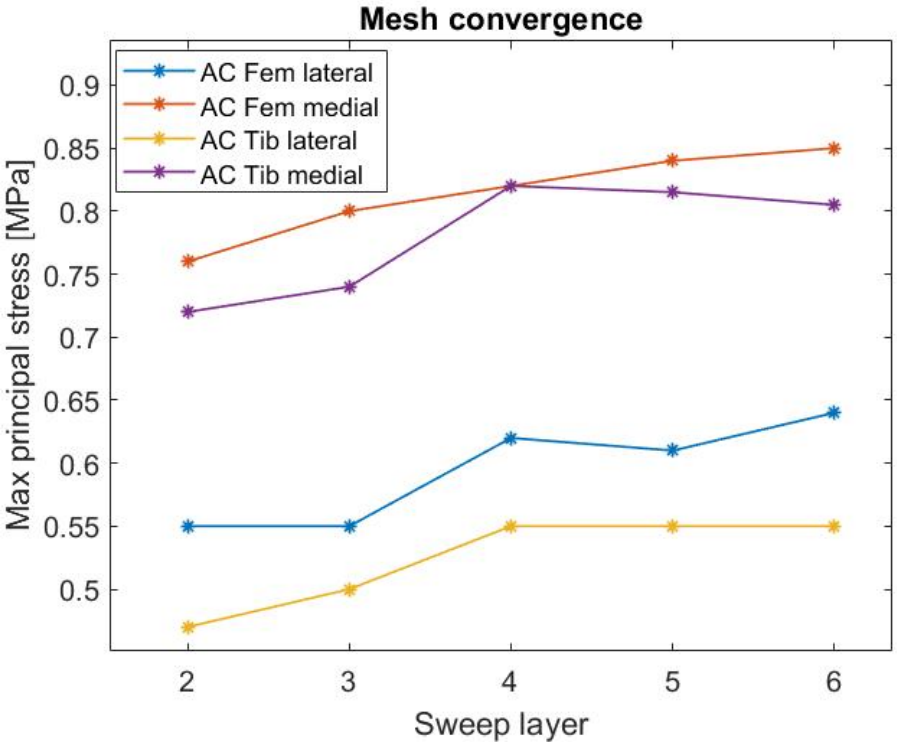

Figure D.1: Results of the mesh convergence study.

E

Appendix: Bone conversion code

```
STLmesh = ['Tibia_2000.stl']
CONVERT_stl_to_sat(STLmesh)

STLmesh = ['Femur_3000.stl']
CONVERT_stl_to_sat(STLmesh)

function CONVERT_stl_to_sat(varargin)
% CONVERT_stl_to_sat  Convert an STL file into ACIS SAT format (v4.0)
%=========================
% FILENAME:           CONVERT_stl_to_sat.m
% AUTHOR:             Adam H. Aitkenhead
% INSTITUTION:        The Christie NHS Foundation Trust
% CONTACT:            adam.aitkenhead@christie.nhs.uk
%=========================

if nargin==0
  error('The <*.stl> input filename is unspecified')
elseif ischar(varargin{1})==0
  error('The <*.stl> input filename must be specified using a string')
elseif nargin==1
  fileIN    = varargin{1};          % Input filename
  STLformat = 'auto';               % Default STL file type (auto-
      detection)
elseif ischar(varargin{2})==0
  error('The STL file type (auto/ascii/binary) must be specified using a
      string')
elseif nargin==2
  fileIN    = varargin{1};          % Input filename
  STLformat = lower(varargin{2});   % STL file type (auto, ascii or binary
      )
elseif nargin>2
  error('Too many input arguments')
end

if exist(fileIN,'file')==0
  error(['The STL file <',fileIN,'> cannot be found'])
end

%=========================
```

```
% Read the STL file
%============================

[coordVERTICES,coordNORMALS] = READ_stl(fileIN,STLformat);

%============================
% Remove any facets containing a zero-length edge
%============================

zeroarealist = max([ min(coordVERTICES(:,:,1)==coordVERTICES(:,:,2),[],2)
    ,...
                     min(coordVERTICES(:,:,2)==coordVERTICES(:,:,3),[],2)
                         ,...
                     min(coordVERTICES(:,:,1)==coordVERTICES(:,:,3),[],2)
                         ,...
                   ],[],2);

coordVERTICES = coordVERTICES(zeroarealist==0,:,:);
coordNORMALS  = coordNORMALS(zeroarealist==0,:,:);

%============================
% Define the output filename
%============================

% Find the '.stl' extension and replace with '.sat' in the output filename
extensionIND = strfind(fileIN,'.');
fileOUT      = [fileIN(1:extensionIND(end)),'sat'];

% If a file by that name already exists, append a number to the filename:
loopFILENAME = 1;
while exist(fileOUT,'file')
  loopFILENAME = loopFILENAME+1;
  fileOUT = [fileIN(1:extensionIND(end)-1),'_',num2str(loopFILENAME),'.sat
      '];
end

%============================
% Write the ACIS SAT file
%============================

[warncodelist] = WRITE_sat(fileOUT,coordVERTICES,coordNORMALS);

%============================
% Display end notes to user
%============================

if sum(warncodelist)>0
  disp(' File conversion failed.')
else
  disp(' File conversion completed.')
end
disp(' ')
end
```

F

Appendix: Degeneration algorithm

```
from caeModules import *
import random
from array import *
from odbAccess import openOdb
import odbAccess
import math
import numpy as np

odb=openOdb('Model.odb')

OdbFull = odb.steps['Gait-cycle'].frames
frames = len(OdbFull)    # Number of frames

# For the current degeneration, the degeneration is calculated per element, for the entire step
Step_time = []    # step time is documented in strings
for t in range(frames):
    Time = OdbFull[t].frameValue
    Step_time.append(Time)

# INC is the duration of the increment
INC =  np.diff(Step_time)

#Threshold values
T_stress5 = 5
T_stress3 = 3

# loop to find the desired element numbers of the instance you want
Fem = []
Tib = []
for i in range(len(OdbFull[0].fieldOutputs['S'].values)):
    if OdbFull[1].fieldOutputs['S'].values[i].instance == None:
      continue
    else:
        Inst= OdbFull[0].fieldOutputs['S'].values[i].instance.name
        if Inst == 'ACFEMUR_1':
            Fem.append(i)    # elements of the desired instance
        elif Inst == 'ACTIBIA_1':
            Tib.append(i)
```

```
39
40 # Extract AC femur max principal stresses
41 Stress_Fem = [[0.0]*frames for i in range(len(Fem))]
42 for f in range(0,frames):
43     CurrentFrame = OdbFull[f].fieldOutputs['S'].values
44     for e in Fem:
45         MaxS = CurrentFrame[e].maxPrincipal
46         i = e - Fem[0]
47         Stress_Fem[i][f] = MaxS
48
49 ## calculate CARTILAGE DEGENERATION for Femur
50 Fem_t5 =[]
51 Deg5 = []
52 for e in range(len(Fem)):
53     Sel = Stress_Fem[e]
54     for f in range(0,frames):
55         Sel_t = abs(Sel[f])    # absolute values as T_stress is based on
               compression stress, which is negative direction
56         if Sel_t > T_stress5:
57             D5 = ((Sel_t - T_stress5)/T_stress5)/100     # calculate the
                   degeneration factor
58             Deg5.append(D5)
59         elif Sel_t <= T_stress5:
60             D5 = 0
61             Deg5.append(D5)
62     Fem_t5.append(Deg5)
63     Deg5 = []
64
65 Deg_Fem5 =[]
66 for e in range(len(Fem)):
67     Del5 = Fem_t5[e]
68     Deg_el5 = 1 - ((sum(Del5[1:]*INC))**(1/1.5))              # Skip the 0
           degeneration at timestep 0
69     Deg_Fem5.append(Deg_el5)
70     Deg_el5=[]
71
72 Fem_t3 =[]
73 Deg3 = []
74 for e in range(len(Fem)):
75     Sel = Stress_Fem[e]
76     for f in range(0,frames):
77         Sel_t = abs(Sel[f])    # absolute values as T_stress is based on
               compression stress, which is negative direction
78         if Sel_t > T_stress3:
79             D3 = ((Sel_t - T_stress3)/T_stress3)/100     # calculate the
                   degeneration factor
80             Deg3.append(D3)
81         elif Sel_t <= T_stress3:
82             D3 = 0
83             Deg3.append(D3)
84     Fem_t3.append(Deg3)
85     Deg3 = []
86
87 Deg_Fem3 =[]
88 for e in range(len(Fem)):
89     Del3 = Fem_t3[e]
```

```
90      Deg_el3 = 1 - ((sum(Del3[1:]*INC))**(1/1.5))                # Skip the 0
            degeneration at timestep 0
91      Deg_Fem3.append(Deg_el3)
92      Deg_el3=[]
93
94  ## Tibial stresses
95  # Extract AC Tibia max principal stresses
96  Stress_Tib = [[0.0]*frames for i in range(len(Tib))]
97  for f in range(0,frames):
98      CurrentFrame = OdbFull[f].fieldOutputs['S'].values
99      for e in Tib:
100         MaxS = CurrentFrame[e].maxPrincipal
101         i = e - Tib[0]
102         Stress_Tib[i][f] = MaxS
103
104 ## calculate CARTILAGE DEGENERATION for Tibia
105 Tib_t5 =[]
106 for e in range(len(Tib)):
107     Sel = Stress_Tib[e]
108     for f in range(0,frames):
109         Sel_t = abs(Sel[f])    # absolute values as T_stress is based on
                compression stress, which is negative direction
110         if Sel_t > T_stress5:
111             D5 = ((Sel_t - T_stress5)/T_stress5)/100     # calculate the
                    degeneration factor
112             Deg5.append(D5)
113         elif Sel_t <= T_stress5:
114             D5 = 0
115             Deg5.append(D5)
116     Tib_t5.append(Deg5)
117     Deg5 = []
118
119 Deg_Tib5 =[]
120 for e in range(len(Tib)):
121     Del5 = Tib_t5[e]
122     Deg_el5 = 1 - ((sum(Del5[1:]*INC))**(1/1.5))                # Skip the 0
            degeneration at timestep 0
123     Deg_Tib5.append(Deg_el5)
124     Deg_el5=[]
125
126 Tib_t3 =[]
127 for e in range(len(Tib)):
128     Sel = Stress_Tib[e]
129     for f in range(0,frames):
130         Sel_t = abs(Sel[f])    # absolute values as T_stress is based on
                compression stress, which is negative direction
131         if Sel_t > T_stress3:
132             D3 = ((Sel_t - T_stress3)/T_stress3)/100     # calculate the
                    degeneration factor
133             Deg3.append(D3)
134         elif Sel_t <= T_stress3:
135             D3 = 0
136             Deg3.append(D3)
137     Tib_t3.append(Deg3)
138     Deg3 = []
139
```

```
140 Deg_Tib3 =[]
141 for e in range(len(Tib)):
142     Del3 = Tib_t3[e]
143     Deg_el3 = 1 - ((sum(Del3[1:]*INC))**(1/1.5))              # Skip the 0
            degeneration at timestep 0
144     Deg_Tib3.append(Deg_el3)
145     Deg_el3=[]
146
147 # For Matlab analysis, I should get the coordinates for de elements
148 Fem_x = []
149 Fem_y = []
150 Fem_z = []
151 Fem_Co = []
152 for e in range(len(Fem)):
153     El_nodes = mdb.models['Model'].parts['ACFEMUR'].elements[e].
            connectivity
154     Node_co1 = mdb.models['Model'].parts['ACFEMUR'].nodes[El_nodes[0]].
            coordinates
155     Node_co2 = mdb.models['Model'].parts['ACFEMUR'].nodes[El_nodes[1]].
            coordinates
156     Node_co3 = mdb.models['Model'].parts['ACFEMUR'].nodes[El_nodes[2]].
            coordinates
157     Node_co4 = mdb.models['Model'].parts['ACFEMUR'].nodes[El_nodes[3]].
            coordinates
158
159     Co_x = [Node_co1[0], Node_co2[0],Node_co3[0],Node_co4[0]]
160     mean_x = np.mean(Co_x)
161     Fem_x.append(mean_x)
162     Co_y = [Node_co1[1], Node_co2[1],Node_co3[1],Node_co4[1]]
163     mean_y = np.mean(Co_y)
164     Fem_y.append(mean_y)
165     Co_z = [Node_co1[2], Node_co2[2],Node_co3[2],Node_co4[2]]
166     mean_z = np.mean(Co_z)
167     Fem_z.append(mean_z)
168     Fem_co = [Fem_x[e],Fem_y[e],Fem_z[e]]
169     Fem_Co.append(Fem_co)
170
171 Tib_x = []
172 Tib_y = []
173 Tib_z = []
174 Tib_Co = []
175 for e in range(len(Tib)):
176     El_nodes = mdb.models['Model'].parts['ACTIBIA'].elements[e].
            connectivity
177     Node_co1 = mdb.models['Model'].parts['ACTIBIA'].nodes[El_nodes[0]].
            coordinates
178     Node_co2 = mdb.models['Model'].parts['ACTIBIA'].nodes[El_nodes[1]].
            coordinates
179     Node_co3 = mdb.models['Model'].parts['ACTIBIA'].nodes[El_nodes[2]].
            coordinates
180     Node_co4 = mdb.models['Model'].parts['ACTIBIA'].nodes[El_nodes[3]].
            coordinates
181
182     Co_x = [Node_co1[0], Node_co2[0],Node_co3[0],Node_co4[0]]
183     mean_x = np.mean(Co_x)
184     Tib_x.append(mean_x)
```

```
185         Co_y = [Node_co1[1], Node_co2[1],Node_co3[1],Node_co4[1]]
186         mean_y = np.mean(Co_y)
187         Tib_y.append(mean_y)
188         Co_z = [Node_co1[2], Node_co2[2],Node_co3[2],Node_co4[2]]
189         mean_z = np.mean(Co_z)
190         Tib_z.append(mean_z)
191         Tib_co = [Tib_x[e],Tib_y[e],Tib_z[e]]
192         Tib_Co.append(Tib_co)
193
194 odb.save()
195 odb.close()
```

G

Appendix: DHPC

Running the FE knee model with the degeneration algorithm in the DHPC was done by submitting the following batch file;

```
#!/bin/sh
#SBATCH --job-name="abaqus"
#SBATCH --partition=compute
#SBATCH --nodes=1
#SBATCH --ntasks-per-node=1
#SBATCH --cpus-per-task=10
#SBATCH --time=24:00:00
#SBATCH --mem-per-cpu=10G
#SBATCH --account=education-3me-msc-be

module load abaqus

abq2022 cpus=$SLURM_NPROCS mp_mode=threads job=Model cpus=10
    interactive

abq2022 cae noGUI=Degeneration_algorithm.py
```

The 'Model' file is the .inp (input) file containing the code for the model to be submitted. The .py file contains the degeneration algorithm to be implemented.

Access to the visual node was achieved by running the following lines on the DHPC start-up node to:

```
module load 2022r2
module load desktop
module load slurm
vnc_desktop 1h -- --cpus-per-task=8 --mem-per-cpu=8GB
```

Tiger VNC (Version 2) was used as a remote display system for visualization of the virtual desktop environment of the DHPC. In the environment, Abaqus was accessed by running the following lines:

```
module load 2022r2
module load visual
module load qt
module load abaqus
module load virtualgl
vglrun abq cae
```

Appendix: Outliers

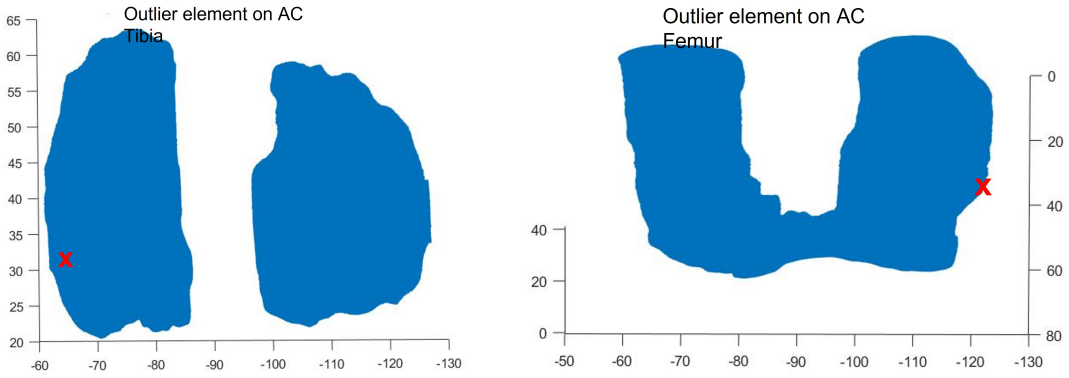

(a) Outlier element on the AC tibia

(b) Outlier element on the AC femur

Figure H.1: Outlier elements that were excluded from the data sets.

Appendix: Figures of degeneration

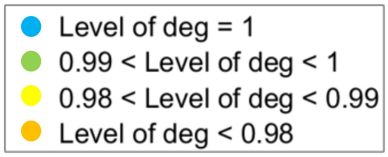

(a) Legend

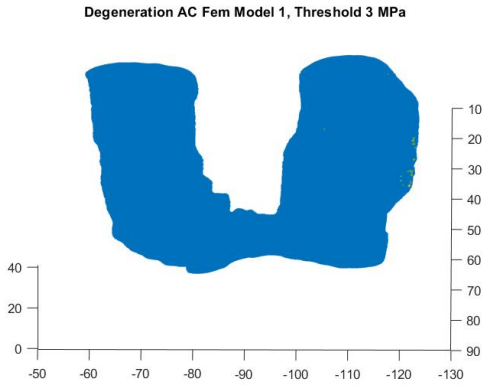

(b) AC femur superior view
Model 1, AC: 5 MPa, menisci: 59 MPa

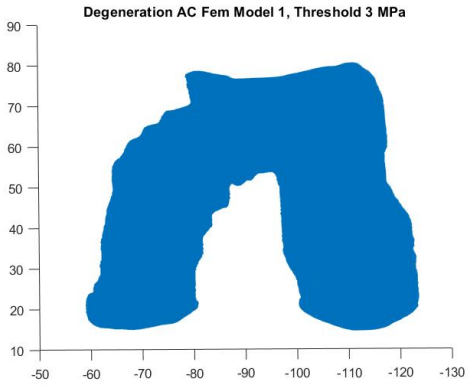

(c) AC femur inferior view
Model 1, AC: 5 MPa, menisci: 59 MPa

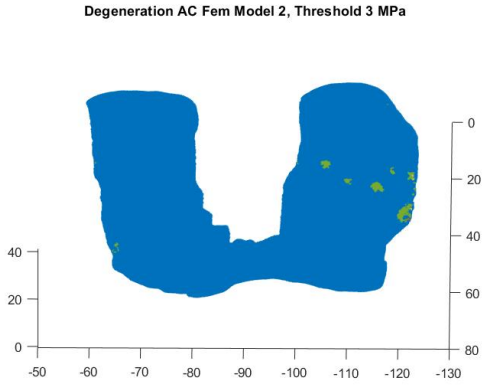

(d) AC femur superior view
Model 2, AC: 11 MPa, menisci: 59 MPa

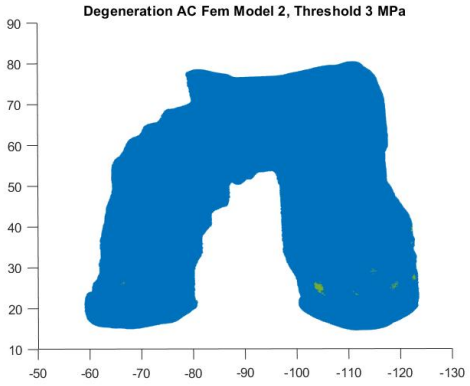

(e) AC femur inferior view
Model 2, AC: 11 MPa, menisci: 59 MPa

Figure I.1: Level of degeneration mapped over the AC femur, left-right: medial-lateral condyle

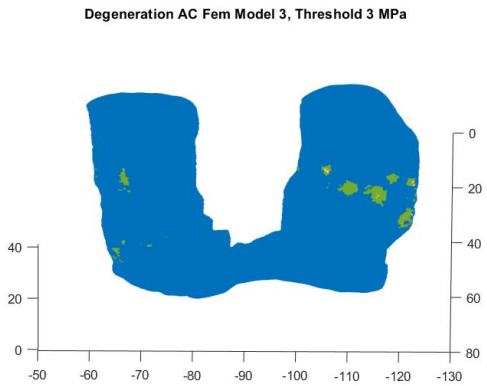

(a) AC femur superior view
Model 3, AC: 17 MPa, menisci: 59 MPa

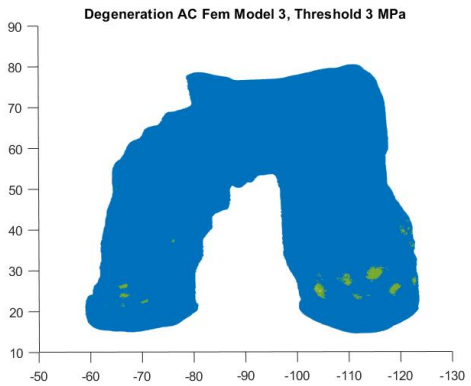

(b) AC femur inferior view
Model 3, AC: 17 MPa, menisci: 59 MPa

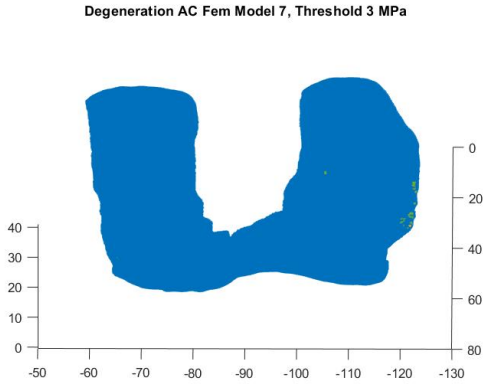

(c) AC femur superior view
Model 7, AC: 5 MPa, menisci: 66 MPa

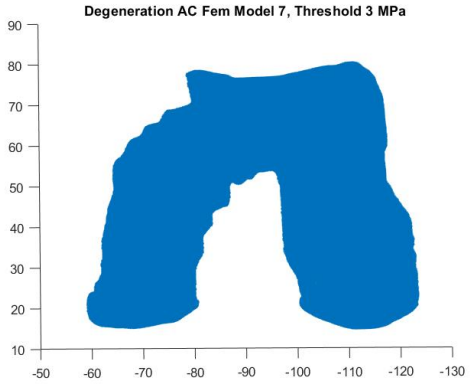

(d) AC femur inferior view
Model 7, AC: 5 MPa, menisci: 66 MPa

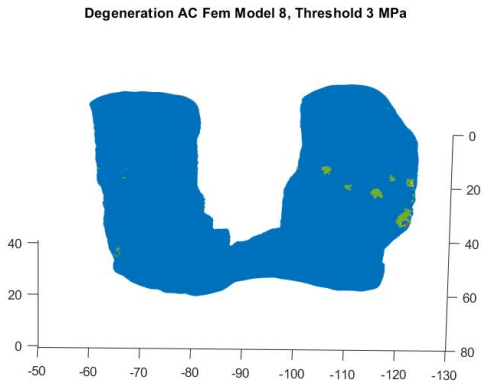

(e) AC femur superior view
Model 8, AC: 11 MPa, menisci: 66 MPa

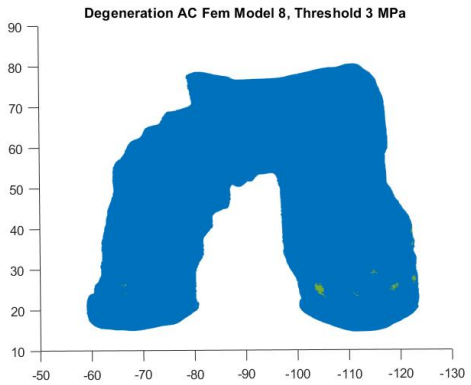

(f) AC femur inferior view
Model 8, AC: 11 MPa, menisci: 66 MPa

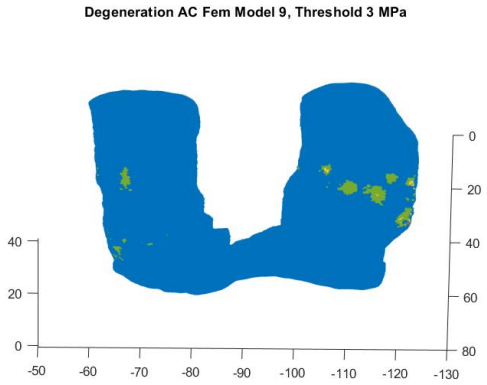

(g) AC femur superior view
Model 9, AC: 17 MPa, menisci: 66 MPa

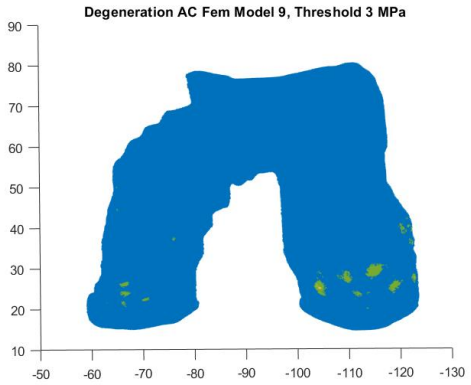

(h) AC femur inferior view
Model 9, AC: 17 MPa, menisci: 66 MPa

Figure I.2: Continuation: Level of degeneration mapped over the AC femur, left-right: medial-lateral condyle

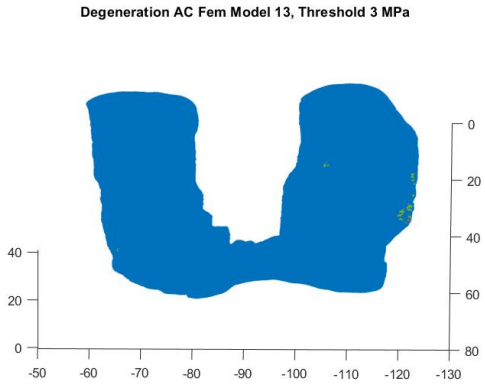

(a) AC femur superior view
Model 13, AC: 5 MPa, menisci: 73 MPa

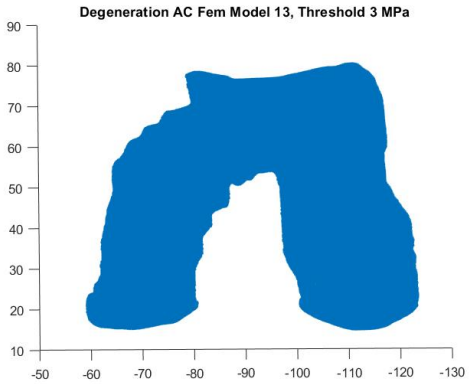

(b) AC femur inferior view
Model 13, AC: 5 MPa, menisci: 73 MPa

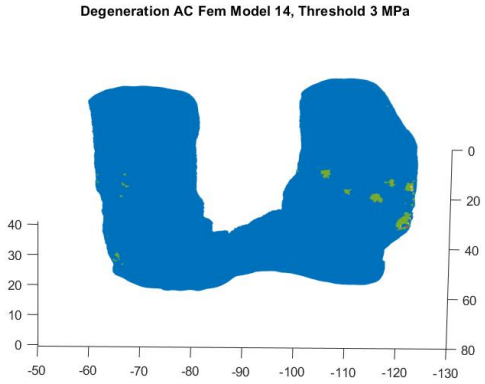

(c) AC femur superior view
Model 14, AC: 11 MPa, menisci: 73 MPa

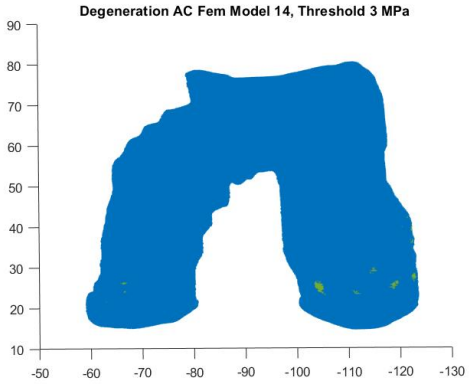

(d) AC femur inferior view
Model 14, AC: 11 MPa, menisci: 73 MPa

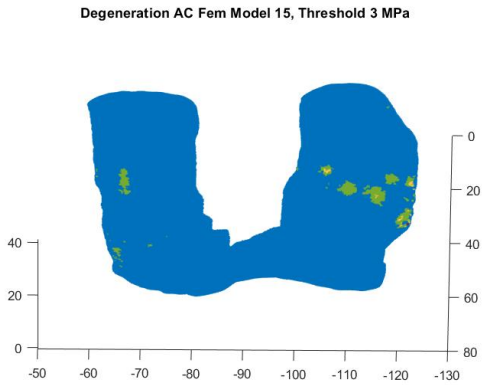

(e) AC femur superior view
Model 15, AC: 17 MPa, menisci: 73 MPa

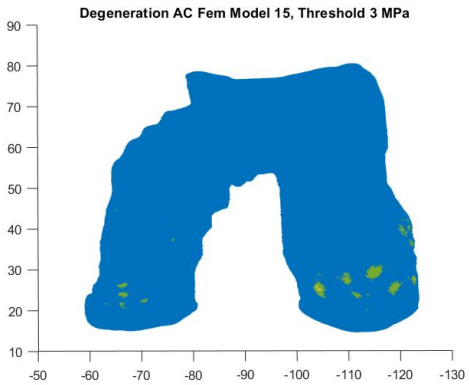

(f) AC femur inferior view
Model 15, AC: 17 MPa, menisci: 73 MPa

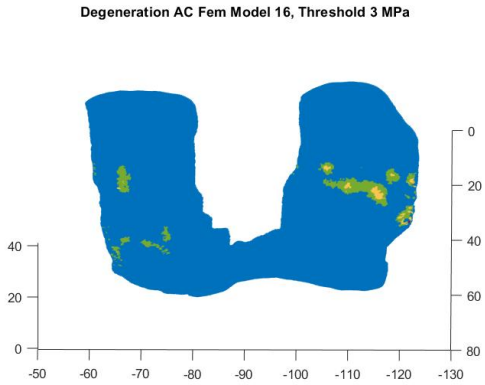

(g) AC femur superior view
Model 16, AC: 23 MPa, menisci: 73 MPa

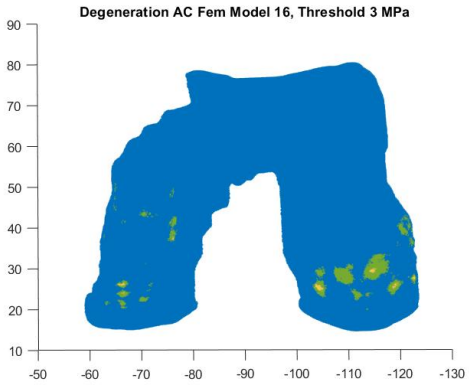

(h) AC femur inferior view
Model 16, AC: 23 MPa, menisci: 73 MPa

Figure I.3: Continuation: Level of degeneration mapped over the AC femur, left-right: medial-lateral condyle

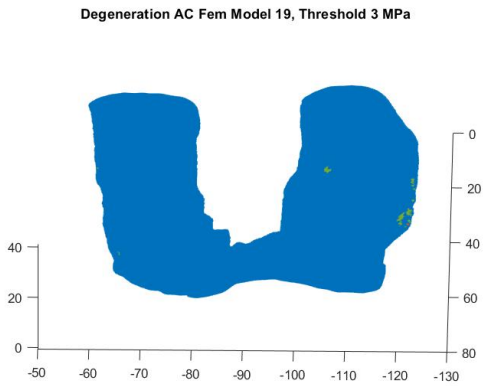

(a) AC femur superior view
Model 19, AC: 5 MPa, menisci: 80 MPa

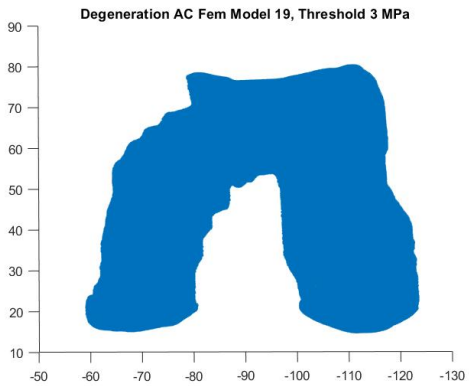

(b) AC femur inferior view
Model 19, AC: 5 MPa, menisci: 80 MPa

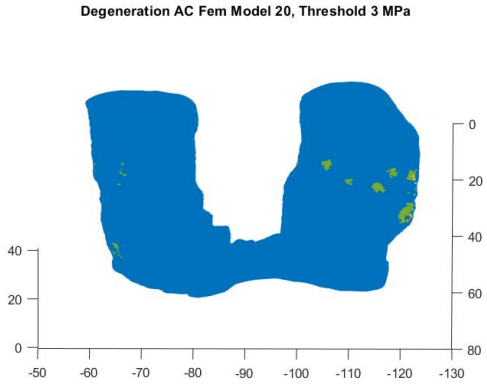

(c) AC femur superior view
Model 20, AC: 11 MPa, menisci: 80 MPa

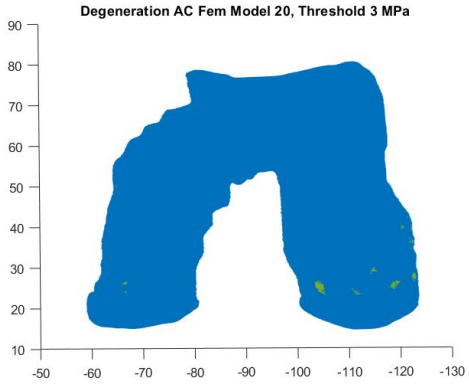

(d) AC femur inferior view
Model 20, AC: 11 MPa, menisci: 80 MPa

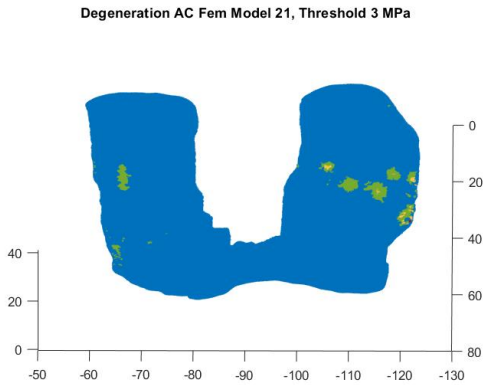

(e) AC femur superior view
Model 21, AC: 17 MPa, menisci: 80 MPa

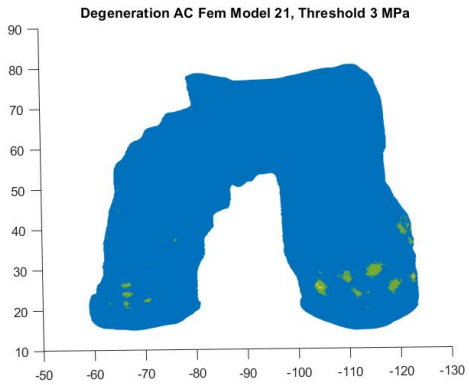

(f) AC femur inferior view
Model 21, AC: 17 MPa, menisci: 80 MPa

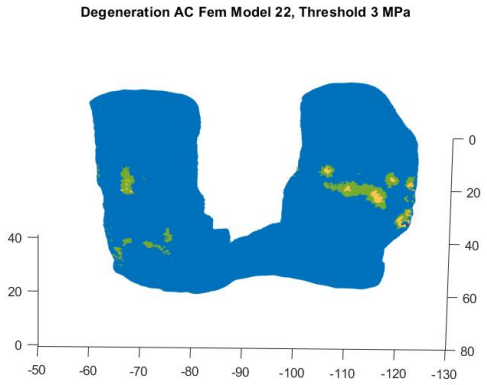

(g) AC femur superior view
Model 22, AC: 23 MPa, menisci: 80 MPa

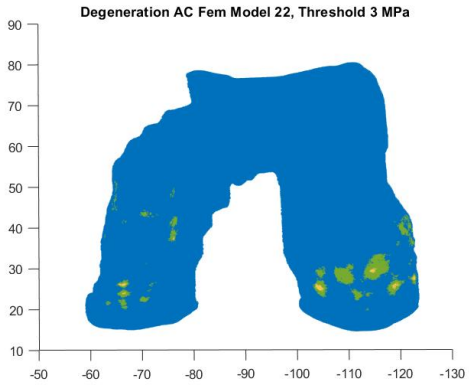

(h) AC femur inferior view
Model 22, AC: 23 MPa, menisci: 80 MPa

Figure I.4: Continuation: Level of degeneration mapped over the AC femur, left-right: medial-lateral condyle

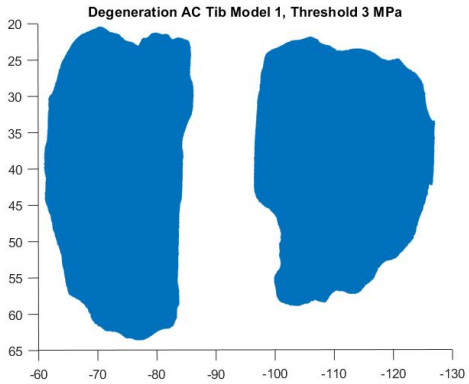

(a) AC tibia superior view
Model 1, AC: 5 MPa, menisci: 59 MPa

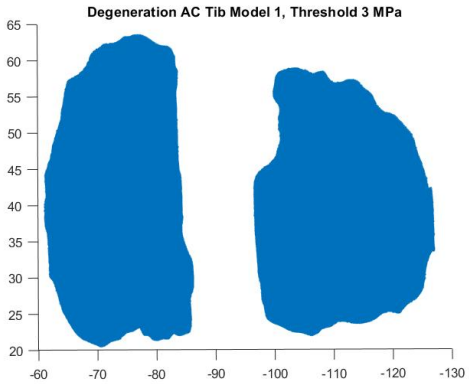

(b) AC tibia inferior view
Model 1, AC: 5 MPa, menisci: 59 MPa

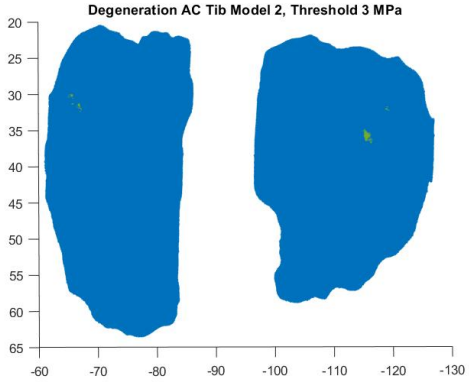

(c) AC tibia superior view
Model 2, AC: 11 MPa, menisci: 59 MPa

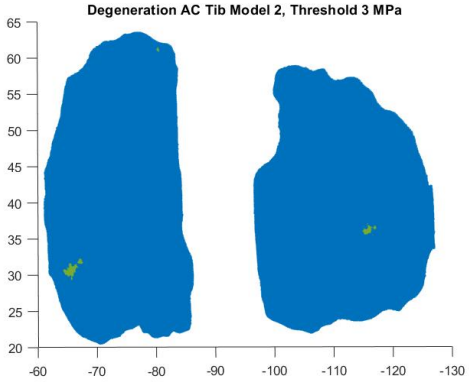

(d) AC tibia inferior view
Model 2, AC: 11 MPa, menisci: 59 MPa

Figure I.5: Level of degeneration mapped over the AC tibia, left-right: medial-lateral condyle

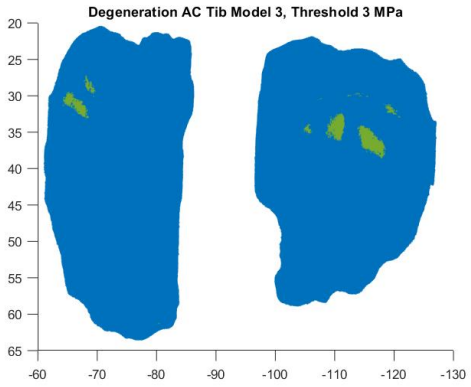

(a) AC tibia superior view
Model 3, AC: 17 MPa, menisci: 59 MPa

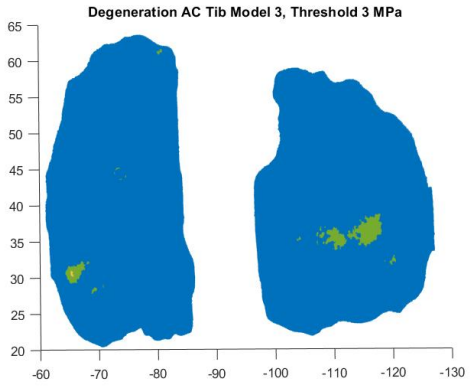

(b) AC tibia inferior view
Model 3, AC: 17 MPa, menisci: 59 MPa

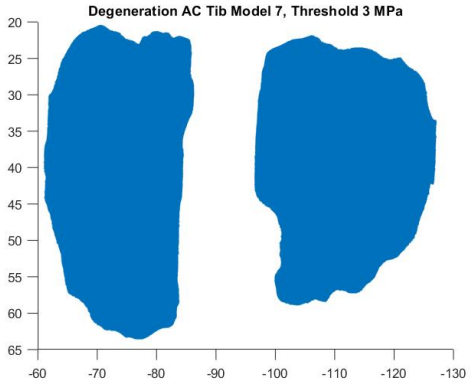

(c) AC tibia superior view
Model 7, AC: 5 MPa, menisci: 66 MPa

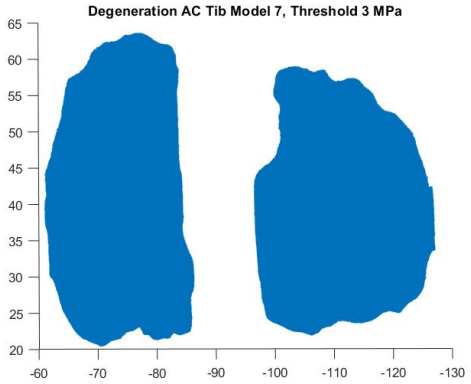

(d) AC tibia inferior view
Model 7, AC: 5 MPa, menisci: 66 MPa

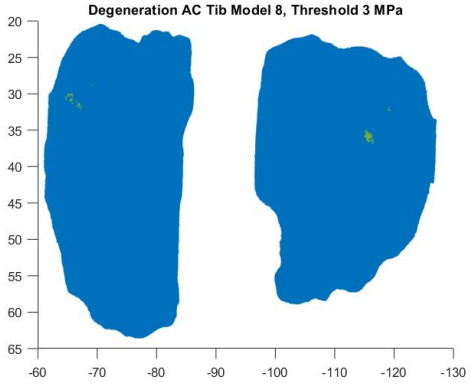

(e) AC tibia superior view
Model 8, AC: 11 MPa, menisci: 66 MPa

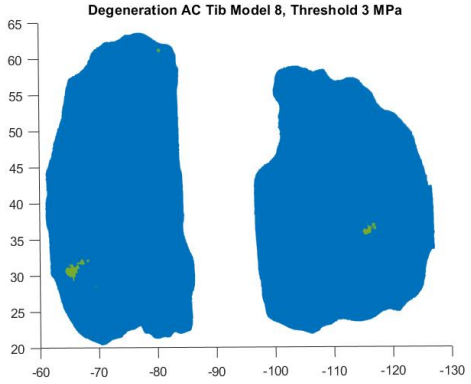

(f) AC tibia inferior view
Model 8, AC: 11 MPa, menisci: 66 MPa

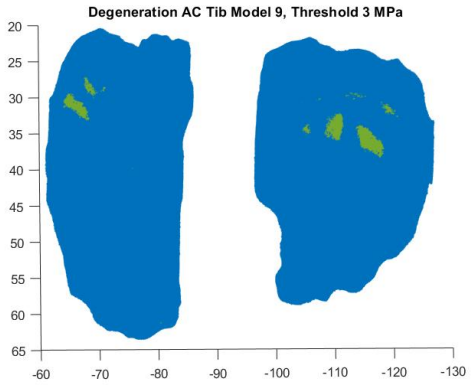

(g) AC tibia superior view
Model 9, AC: 17 MPa, menisci: 66 MPa

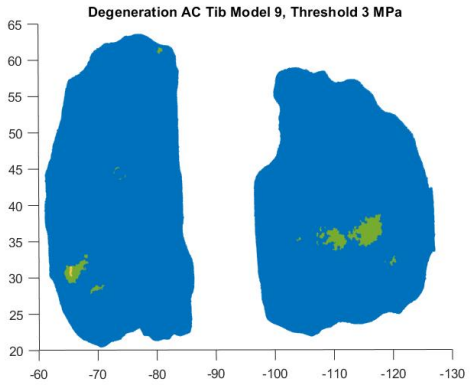

(h) AC tibia inferior view
Model 9, AC: 17 MPa, menisci: 66 MPa

Figure I.6: Continuation: Level of degeneration mapped over the AC tibia, left-right: medial-lateral condyle

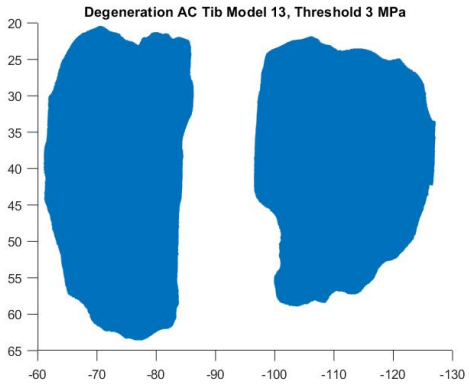

(a) AC tibia superior view
Model 13, AC: 5 MPa, menisci: 73 MPa

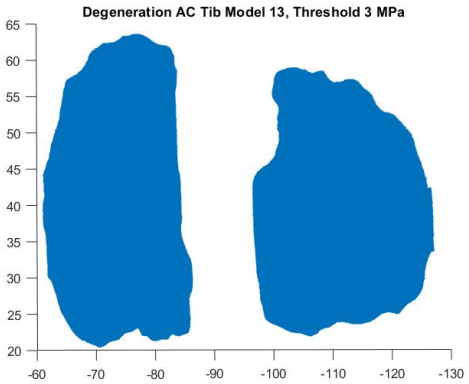

(b) AC tibia inferior view
Model 13, AC: 5 MPa, menisci: 73 MPa

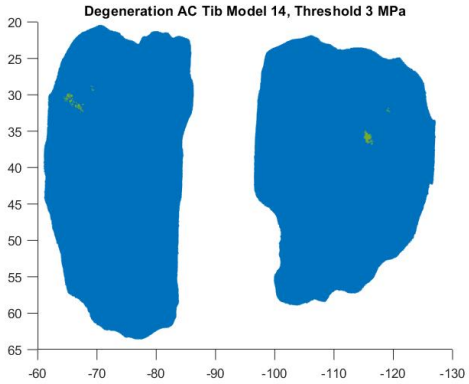

(c) AC tibia superior view
Model 14, AC: 11 MPa, menisci: 73 MPa

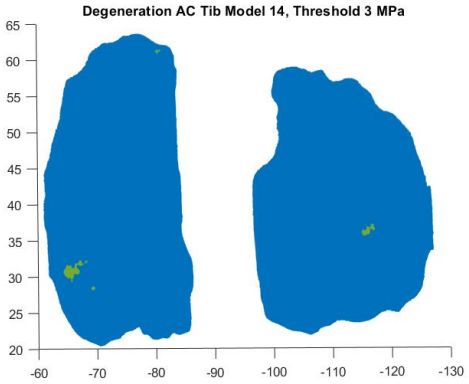

(d) AC tibia inferior view
Model 14, AC: 11 MPa, menisci: 73 MPa

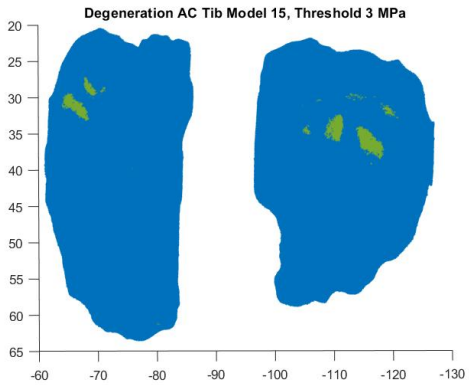

(e) AC tibia superior view
Model 15, AC: 17 MPa, menisci: 73 MPa

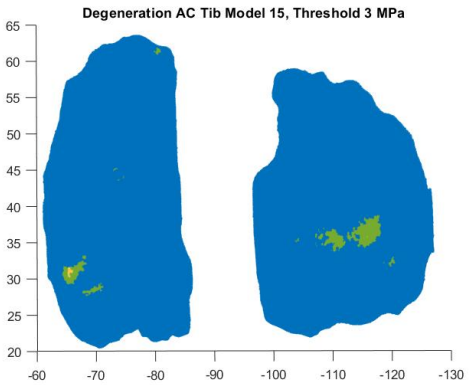

(f) AC tibia inferior view
Model 15, AC: 17 MPa, menisci: 73 MPa

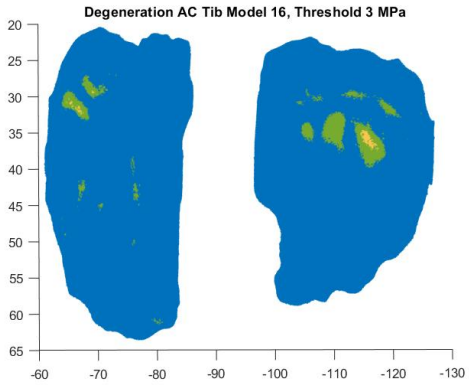

(g) AC tibia superior view
Model 16, AC: 23 MPa, menisci: 73 MPa

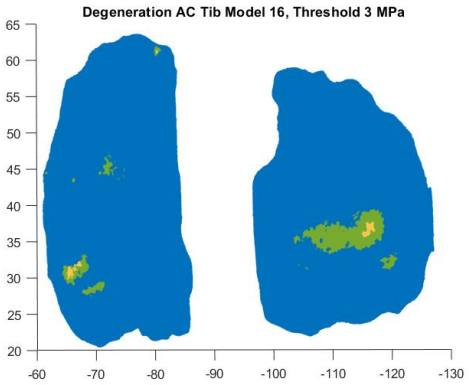

(h) AC tibia inferior view
Model 16, AC: 23 MPa, menisci: 73 MPa

Figure I.7: Continuation: Level of degeneration mapped over the AC tibia, left-right: medial-lateral condyle

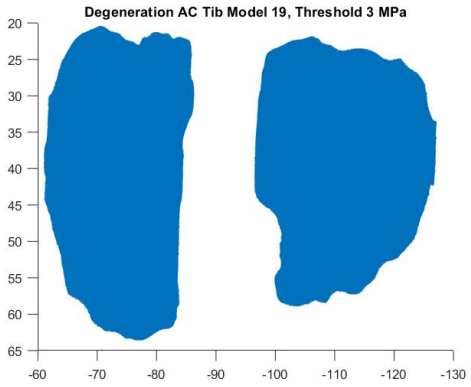

(a) AC tibia superior view
Model 19, AC: 5 MPa, menisci: 80 MPa

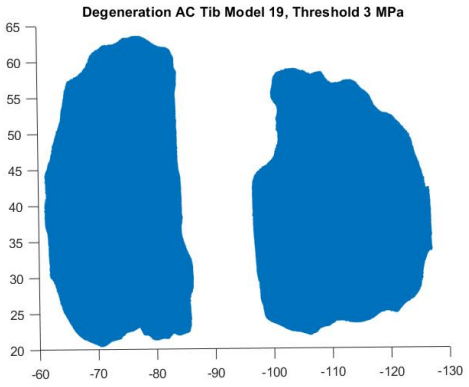

(b) AC tibia inferior view
Model 19, AC: 5 MPa, menisci: 80 MPa

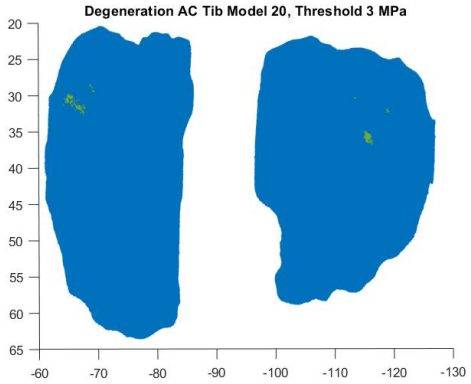

(c) AC tibia superior view
Model 20, AC: 11 MPa, menisci: 80 MPa

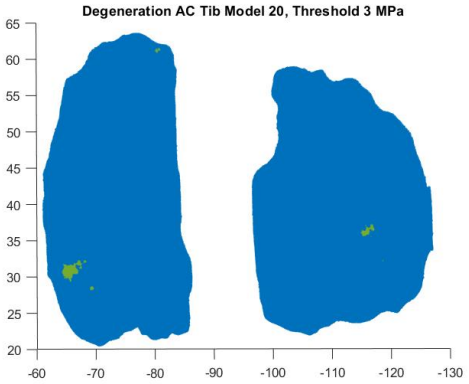

(d) AC tibia inferior view
Model 20, AC: 11 MPa, menisci: 80 MPa

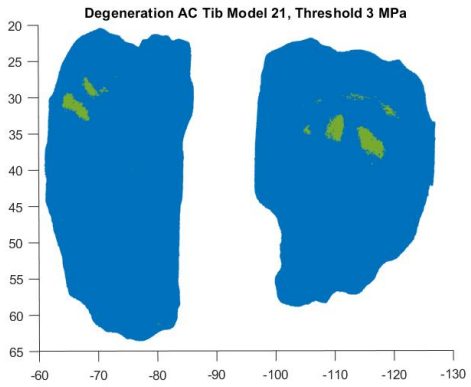

(e) AC tibia superior view
Model 21, AC: 17 MPa, menisci: 80 MPa

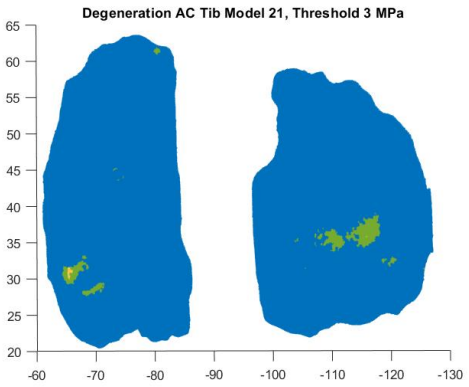

(f) AC tibia inferior view
Model 21, AC: 17 MPa, menisci: 80 MPa

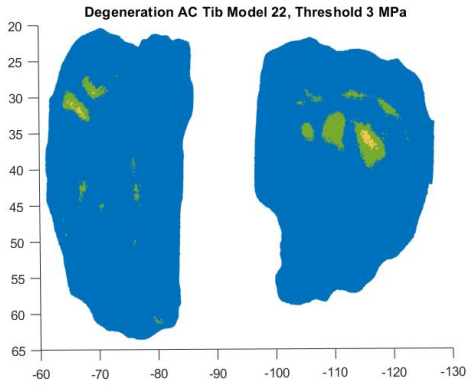

(g) AC tibia superior view
Model 22, AC: 23 MPa, menisci: 80 MPa

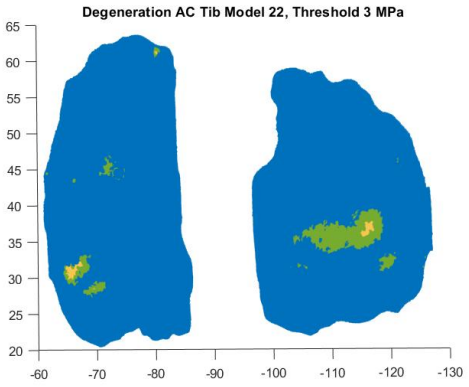

(h) AC tibia inferior view
Model 22, AC: 23 MPa, menisci: 80 MPa

Figure I.8: Continuation: Level of degeneration mapped over the AC tibia, left-right: medial-lateral condyle